Decadal Variability of the Indian and Pacific Walker Cells since the 1960s: Do They Covary on Decadal Time Scales?

WEIQING HAN,[a] GERALD A. MEEHL,[b] AIXUE HU,[b] JIAN ZHENG,[c] JESSICA KENIGSON,[a] JÉRÔME VIALARD,[d] BALAJI RAJAGOPALAN,[e] AND YANTO[f]

[a] *Department of Atmospheric and Oceanic Sciences, University of Colorado Boulder, Boulder, Colorado*
[b] *Climate and Global Division, National Center for Atmospheric Research, Boulder, Colorado*
[c] *Institute of Oceanology, Chinese Academy of Sciences, Qingdao, China*
[d] *Laboratoire d'Océanographie: Expérimentation et Approches Numériques, IPSL, Sorbonne Universités/UPMC, IRD, CNRS, MNHN, Paris, France*
[e] *Department of Civil, Environmental, and Architectural Engineering, University of Colorado Boulder, Boulder, Colorado*
[f] *Department of Civil Engineering, Jenderal Soedirman University, Purwokerto, Indonesia*

(Manuscript received 31 October 2016, in final form 7 July 2017)

ABSTRACT

Previous studies have investigated the centennial and multidecadal trends of the Pacific and Indian Ocean Walker cells (WCs) during the past century, but have obtained no consensus owing to data uncertainties and weak signals of the long-term trends. This paper focuses on decadal variability (periods of one to few decades) by first documenting the variability of the WCs and warm-pool convection, and their covariability since the 1960s, using in situ and satellite observations and reanalysis products. The causes for the variability and covariability are then explored using a Bayesian dynamic linear model, which can extract nonstationary effects of climate modes. The warm-pool convection exhibits apparent decadal variability, generally covarying with the Indian and Pacific Ocean WCs during winter (November–April) with enhanced convection corresponding to intensified WCs, and the Indian–Pacific WCs covary. During summer (May–October), the warm-pool convection still highly covaries with the Pacific WC but does not covary with the Indian Ocean WC, and the Indian–Pacific WCs are uncorrelated. The wintertime coherent variability results from the vital influence of ENSO decadal variation, which reduces warm-pool convection and weakens the WCs during El Niño–like conditions. During summer, while ENSO decadal variability still dominates the Pacific WC, decadal variations of ENSO, the Indian Ocean dipole, Indian summer monsoon convection, and tropical Indian Ocean SST have comparable effects on the Indian Ocean WC overall, with monsoon convection having the largest effect since the 1990s. The complex causes for the Indian Ocean WC during summer result in its poor covariability with the Pacific WC and warm-pool convection.

1. Introduction

The Indian and Pacific Ocean Walker cells (WCs), sometimes referred to as the western and eastern Walker cells respectively (Meehl and Arblaster 2002; Meehl et al. 2003), are equatorial zonal atmospheric circulation cells driven by atmospheric deep convection over the Indo-Pacific warm-pool region (Fig. 1; Walker and Bliss 1937) and modified by various ocean–atmosphere feedback processes (Dijkstra and Neelin 1995). The lower branch of the Pacific WC is associated with equatorial easterly wind, and that of the Indian Ocean WC is on annual average associated with equatorial westerly wind. They converge to the deep convective region over the maritime continents that reside in the Indo-Pacific warm pool (Figs. 1 and 2). Given the intrinsic linkage between convection and WCs, an intriguing question arises: Do the Indo-Pacific WCs covary on decadal time scales, and do they vary with the warm-pool convection?

a. Background

On interannual time scale, observational analyses show that variability of the Indian and Pacific Ocean WCs is a fundamental element of the tropospheric biennial oscillation (TBO) of the Indian–Australian monsoon (e.g., Meehl and Arblaster 2002; Meehl et al. 2003). The TBO involves El Niño–Southern Oscillation (ENSO) and the Indian Ocean dipole (IOD; Saji et al.

Corresponding author: Weiqing Han, weiqing.han@colorado.edu

DOI: 10.1175/JCLI-D-16-0783.1

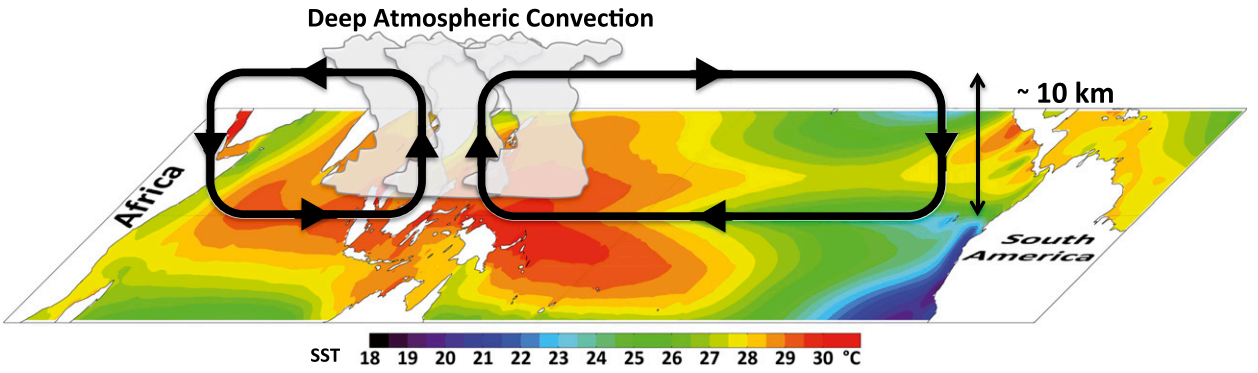

FIG. 1. Schematic diagram of the Indian and Pacific Ocean WCs. The ascending branch over warm water is associated with low surface pressure and the descending branches over cold water are associated with high surface pressure. Adapted from Han et al. (2014a).

1999; Webster et al. 1999), the two most prominent interannual climate modes over the tropical Indo-Pacific basin that are associated with variability of the Indian and Pacific Ocean WCs (Meehl and Arblaster 2002; Meehl et al. 2003). There is significant covariability between the Indian and Pacific Ocean WCs, which may result partly from co-occurrence of ENSO and the IOD (e.g., Allan et al. 2001; Baquero-Bernal et al. 2002; Xie et al. 2002; Hastenrath 2002; Krishnamurthy and Kirtman 2003; Annamalai et al. 2003), particularly after 1976 (Annamalai et al. 2005), with El Niño tending to excite a positive IOD and therefore yielding weakened Pacific and Indian Ocean WCs. ENSO and IOD, however, can sometimes operate independently (e.g., Yamagata et al. 2003; Sun et al. 2015), during which times the Indian and Pacific Ocean WCs do not necessarily covary.

On multidecadal and centennial time scales, trend analyses of the Indian and Pacific Ocean WCs have been carried out, using surface observations and reanalysis data to infer changes in the WC strength. Yet no consensus has been reached. Observational studies provide contrasting results, depending on the datasets and techniques used in the analyses. Over the Pacific Ocean, several observational studies have argued for weakened zonal sea level pressure (SLP) and sea surface temperature (SST) gradients and a slowdown of the surface easterlies, and therefore a weaker WC since the mid-nineteenth century, during the twentieth century and since 1950 (Vecchi and Soden 2007; Deser et al. 2010; Tokinaga et al. 2012a,b, Yasunaka and Kimoto 2013). By contrast, other studies suggest enhanced trends in equatorial Pacific zonal SST gradients over the past century (Karnauskas et al. 2009), particularly after ENSO signals are removed (Solomon and Newman 2012); however, there is no robust strengthening or weakening trend in zonal SLP gradient and therefore the WC (Solomon and Newman 2012). An enhanced zonal SLP gradient and intensified WC over the Pacific since 1950 have also been suggested (L'Heureux et al. 2013; Newman 2013). Over the Indian Ocean, there is also no clear agreement on the long-term evolution of equatorial westerlies and WC strength. Atmospheric reanalysis products suggest a strengthening of surface equatorial westerlies and thus stronger WC since the 1950s and 1960s (Han et al. 2010; Yu and Zwiers 2010, Yasunaka and Kimoto 2013), whereas the bias-corrected observed winds indicate a weakening of surface westerlies and therefore weaker WC for similar temporal periods (Tokinaga et al. 2012a,b).

Modeling studies also provide inconsistent results. Coupled global climate models have produced a robust slowdown trend of the tropical atmospheric circulation since the mid-nineteenth century and in the projected twenty-first century, particularly the Pacific WC (e.g., Vecchi et al. 2006; Vecchi and Soden 2007; Chadwick et al. 2013) and the Asian monsoon circulation (but with enhanced monsoon rainfall; Turner and Annamalai 2012; Kitoh et al. 2013), in response to increasing greenhouse gas forcing. However, the limited ability of the models to simulate the present monsoon change and the large spread among the model projections limit our confidence in the results (e.g., Kitoh et al. 2013). Standalone atmospheric general circulation models simulated inconsistent changes in the WC strength depending on which SST product was used to force the models: Using HadISST of Rayner et al. (2006) produced a strengthened Indo-Pacific WC for the twentieth century and since 1950, using the Extended Reconstructed SST of Smith and Reynolds (2004) generated a neutral response, and using Hadley Centre SST, version 3 (HadSST3), of Kennedy et al. (2011a,b) produced a weakened WC (see Tokinaga et al. 2012a; Meng et al. 2012).

The lack of consensus in both observational and modeling studies may arise from many factors, such as

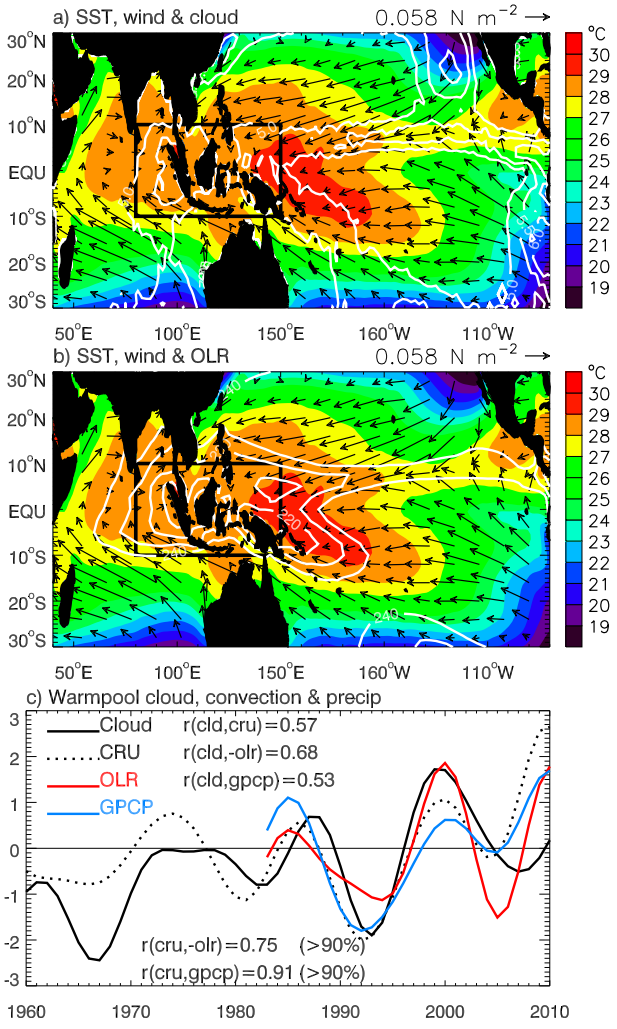

FIG. 2. (a) The 1950–2009 mean SST from HadISST data (color shading; °C), mean cloudiness from ICOADS data (white line contours; okta), and mean surface wind stress (arrows; N m^{-2}) from WASWind data. The boxed region shows the Indo-Pacific warm pool (10°S–10°N, 80°–150°E). Contour interval is 0.5 okta for cloudiness. (b) As in (a), but with the white contours being the 1980–2013 mean OLR (W m^{-2}) from satellite observations; the contour interval is 10 W m^{-2}. (c) Time series of 8-yr low-pass-filtered cloudiness (black solid), CRU precipitation over land (black dotted), −OLR (red), and GPCP precipitation (blue) averaged in the boxed region, where mean cloudiness ≥5 okta as shown in (a) and mean OLR ≤220 W m^{-2} as shown in (b). The first and last four years are excluded from each series to remove the endpoint effect of the filter. For comparison convenience, we show −OLR anomalies in (c). Each curve is normalized by its standard deviation. Correlations above 90% significance are shown in parentheses.

temporal heterogeneity of the observational datasets, differences in analysis methods, and systematic errors in models. These inconsistencies are detrimental to detecting centennial and multidecadal trends because the trend signals are much weaker than the amplitudes of decadal and interdecadal variability over the Indo-Pacific basin (not shown). Therefore, this paper focuses on decadal and interdecadal variability rather than long-term trends. How do the Indian and Pacific Ocean WCs vary on decadal and interdecadal time scales, what are the underlying causes for their variability, and do they covary with the warm-pool convection (Fig. 1)? These are important science issues that have not yet been addressed.

While ENSO and the IOD have been shown to affect interannual variability of the Indian and Pacific Ocean WCs, their effects on decadal time scales remain elusive, even though both ENSO and IOD indices exhibit evident decadal variability (e.g., Ashok et al. 2004; Song et al. 2007; Tozuka et al. 2007). Recent studies suggest that the tropical Indian Ocean warming trend in the past few decades (e.g., Luo et al. 2012; Han et al. 2014b), the Atlantic warming trend and interbasin SST gradient in the past century (Zhang and Karnauskas 2017) and since the early 1990s (Kucharski et al. 2011, 2015; England et al. 2014; McGregor et al. 2014; Li et al. 2016), and the decadal (10–20 yr) Indian Ocean SST variability since the 1980s all have contributed to the intensification of the Pacific WC variability on the corresponding time scales. Additionally, decadal variability of off-equatorial convection associated with the Indian summer monsoon, which can be affected by various factors associated with variability over land and ocean, may also affect the Indian Ocean WC. How these factors affect decadal variability of the Indian and Pacific Ocean WCs, however, is not well known.

b. *Present research*

The goal of this research is to explore the variability of the Indian and Pacific Ocean WCs on time scales of one to a few decades, which we refer to collectively as "decadal variability" hereafter, and to understand the causes. Our period of interest is from the 1960s to the present, when more reliable ocean–atmosphere datasets are available. First, we document the variability of the Indian and Pacific Ocean WCs together with the warm-pool convection, and explore their covariability by analyzing available satellite data, in situ observations, and reanalysis products. Here, we focus on examining the surface branches of the WCs, as in the existing studies that address their centennial and multidecadal trends (see above). Then, we investigate the association of their decadal variability with climate modes and other climate indices, using a novel approach of the Bayesian dynamic linear model (DLM; e.g., Petris et al. 2009) and comparing its results with that of the conventional static linear regression model (SLM). The Bayesian DLM can capture the temporally nonstationary relationship

between the climate indices and the WCs, which cannot be achieved by the SLM (see section 2c).

Results from this study are relevant for understanding past climate variations, improving decadal climate predictions, and setting a process context for longer-term future climate variability and change in the vast Indo-Pacific region. Since little is known about Indian Ocean decadal climate variability and its generation mechanisms (Han et al. 2014a), this study advances our understanding in this aspect. The research will benefit a large percent of the world's population surrounding the tropical Indian and Pacific Oceans as well as around the globe, since changes of the WCs are linked to ENSO and the IOD, which have far-reaching impacts on climate [e.g., Saji et al. 1999; see Wang et al. (2016) for a review and references therein].

2. Data and approach

a. Datasets for detecting decadal variability of Indo-Pacific WCs and warm-pool convection

To document the variability of warm-pool convection, we analyze the monthly cloudiness from 2° × 2° data from the International Comprehensive Ocean–Atmosphere Data Set (ICOADS) available for 1800–2014 (e.g., Woodruff et al. 2011; Freeman et al. 2017) and monthly precipitation over land from the University of East Anglia Climatic Research Unit (CRU) 0.5° × 0.5° data for 1901–2012 (Jones and Harris 2013). To discern whether the cloudiness or precipitation over land can better represent the warm-pool convection for our period of interest from the 1960s onward, we also analyze the satellite-derived 2.5° × 2.5° monthly outgoing longwave radiation (OLR)—a proxy for tropical deep convection—from 1974 to 2013 (Liebmann and Smith 1996), and 2.5° × 2.5° Global Precipitation Climatology Project (GPCP) monthly precipitation from 1979 to 2016 (Adler et al. 2003). The warm-pool region of 10°S–10°N, 80°–150°E (black box of Fig. 2) is chosen because its mean SST is high (≥28°C; color contours of Figs. 2a,b), cloudiness attains its maximum [≥5 okta (1 okta = 1/8); white contours of Fig. 2a], and OLR reaches its minimum (≤220 W m^{-2}; white contours of Fig. 2b). This region shows the WCs' convergence area with convection maximum, and it excludes the intertropical convergence zone and South Pacific convergence zone (Figs. 2a,b).

To understand the seasonality of the warm-pool convection, the time series of convection averaged over the warm-pool region is computed for the annual mean and winter and summer seasons, respectively. In this paper, winter is defined as the November–April mean and summer as the May–October mean. These months are chosen for two reasons: First, November–April corresponds to the wet season and May–October to the dry season over Indonesia (e.g., Yanto et al. 2016), which is within the warm-pool convection region; second, May–October represents the wet season of the Indian summer monsoon. For cloudiness and CRU precipitation averaged over the warm-pool region, their annual (seasonal) means are computed only when nine (four) months or more of valid data are available in that year. Based on this criterion, only 1943 has missing values for cloudiness, which are filled by linear interpolation.

To document the variability of Indian and Pacific Ocean WCs, which are represented by their surface branches defined in section 3a below, we analyze monthly surface wind stress data from the Wave- and Anemometer-Based Sea Surface Wind (WASWind; Tokinaga and Xie 2011) available for 1950–2009, and wind products from the National Centers for Environmental Prediction (NCEP)–National Center for Atmospheric Research (NCAR) reanalysis (Kalnay et al. 1996) for 1948–2013, the Japanese 55-year Reanalysis (JRA-55; Kobayashi et al. 2015) for 1958–2013, and the operational European Centre for Medium-Range Weather Forecasts (ECMWF) ocean reanalysis system (ORAS3) available for 1959–2009, which uses ERA-40 winds before 2002 and numerical weather prediction operational analyses thereafter (Balmaseda et al. 2008). As discussed in section 1, the reanalysis winds show large uncertainty in detecting multidecadal trend since the 1960s. On the other hand, the observation-based WASWind have many missing values over the warm-pool region (see Han et al. 2014b). The monthly surface winds from Cross-Calibrated Multiplatform (CCMP) satellite observations (Atlas et al. 2011; Wentz et al. 2015), version 2.0 (V2.0), since 1987 are also analyzed. This multiple-dataset approach aims to identify signals robust to cross-dataset differences and thus increase the confidence in our analysis.

To further confirm the decadal variability of the Indian and Pacific Ocean WCs detected by surface winds, particularly before the satellite era, we analyze the upper-700-m thermosteric sea level from 1955 to 2013 using yearly *World Ocean Atlas 2013* (*WOA13*) data (Levitus et al. 2012; https://www.nodc.noaa.gov/OC5/woa13/) and from 1945 to 2014 using Ishii and Kimoto (2009) data. They are independent observations from the surface winds. Sea level data from the ORAS4 monthly product (Balmaseda et al. 2013) for 1958–2014, and multiple-satellite merged monthly sea surface height anomalies (SSHA) from the French project Archiving, Validation, and Interpolation of Satellite Oceanographic Data (AVISO) (e.g., Ducet et al. 2000;

Rio et al. 2011) from 1993 to 2014 are also analyzed. Zonal gradients of sea level are calculated, and their variations are compared with those of zonal surface winds that represent the WCs.

The theoretical basis for this analysis is that in the equatorial ocean, decadal variability of zonal surface wind associated with the WCs is a major driver of zonal sea level gradient, and the two are in quasi-steady balance. This can be demonstrated by the zonal momentum equation of a linear, 1.5-layer reduced gravity model on equatorial β plane: $\partial u/\partial t - \beta y v + g'\partial\eta/\partial x = \tau^x/(\rho_0 H)$, where u and v are zonal and meridional current, η is sea level, τ^x is zonal wind stress, g' is reduced gravity parameter, ρ_0 is the mean density of the ocean, and H is the mean layer thickness. The $\partial u/\partial t$ term is small because the decadal time scale is far longer than the equatorial adjustment time scales in the Indian (Han et al. 1999; Shankar et al. 2010) and Pacific Oceans (Jin 2001), which is the time it takes for an equatorial Kelvin wave to cross the basin, and the first meridional mode Rossby wave to return. With Coriolis parameter $f = \beta y = 0$ on the equator and small $\partial u/\partial t$, the equation yields $g\partial\eta/\partial x \approx \tau^x/(\rho_0 H)$, which shows the balance between zonal sea level gradient and zonal wind stress.

To isolate decadal signals, a Lanczos low-pass filter (Duchon 1979) with half power at 8-yr period is used. The response curve of the 8-yr low-pass filter retains approximately 90% of the amplitude at 10-yr period and almost full amplitudes for longer periods, which essentially retain the signals with periods of 10 yr and longer. The 8-yr low-pass filter has been used to investigate the Pacific decadal variability by many previous studies (e.g., Deser et al. 2012).

b. *Datasets for climate modes and other climate indices*

To understand the causes for decadal variations of the Indian and Pacific Ocean WCs and their covariability, we examine their relationships with decadal variability of ENSO and IOD, the two dominant climate modes over the Indo-Pacific basin on interannual time scale. For simplicity, we will refer to decadal variability of ENSO (IOD) simply as ''decadal ENSO (IOD)''. Note that decadal ENSO, represented by 8-yr low-pass-filtered Niño-3.4 index and multivariate ENSO index (MEI), is highly correlated with the interdecadal Pacific oscillation (IPO; e.g., Power et al. 1999; Folland et al. 2002; Meehl and Hu 2006) and the Pacific decadal oscillation (PDO; e.g., Mantua et al. 1997; Minobe 1997; Zhang et al. 1997), with the Niño-3.4–IPO and IPO–PDO correlations being about 0.88 from 1900 to 2008 and the IPO–MEI correlation being 0.89 from 1900 to 2001 (e.g., Zhang and Church 2012; Han et al. 2014b).

For the IOD, its decadal variability is represented by the 8-yr low-pass-filtered dipole mode index (DMI), defined as the difference of SST anomaly (SSTA) between the eastern (10°S–0°N, 90°–110°E) and western (10°S–10°N, 50°–70°E) tropical Indian Ocean (Saji et al. 1999). The DMI exhibits marked interannual variability with decadal modulation (Ashok et al. 2004; Song et al. 2007; Tozuka et al. 2007). While Saji et al. (1999) uses September–November mean DMI to represent the IOD strength, here we calculate the DMI for each month and then compute seasonal and annual means. Consequently, the DMI in this paper essentially represents the east–west SST gradient. For convenience, we still refer it to as the IOD. Indices of ENSO and the IOD are calculated using monthly HadISST data (Rayner et al. 2006) available since 1870.

To examine the possible influence of the Indian and Atlantic Ocean SST variability, we form SST indices by averaging the SSTA over the tropical Indian Ocean (15°S–15°N, 50°–95°E) and the Atlantic Ocean (30°S–60°N, 70°W–20°E) and then perform 8-yr low-pass filtering. These regions are similar to that of Han et al. (2014b) for the Indian Ocean and McGregor et al. (2014) for the Atlantic Ocean that influence the Pacific WC. The Indian Ocean SSTA represents the basinwide warming and cooling associated with ENSO decadal variability (Tozuka et al. 2007), but the association breaks down during recent decades (Han et al. 2014b). To explore the relationship between the Indian summer monsoon and the Indian Ocean WC, the Indian Institute of Tropical Meteorology homogeneous monthly all-India rainfall dataset available from 1871 to 2014 (e.g., Parthasarathy et al. 1995) is analyzed. Time series of all the climate indices are shown in Fig. 3, with the linear trend for their common period of 1962–2009 being removed from each index.

c. *The Bayesian dynamic linear model*

To explore the impacts of the climate modes on decadal variability of the WCs or, more precisely, to assess the WC variability associated with the climate modes, we apply the Bayesian DLM approach. In a conventional SLM, a response variable Y is equated to a linear function of independent predictors $(X_1, \ldots, X_M)$, that is, $Y(t) = b_0 + b_1 X_1(t) + \cdots + b_M X_M(t) + \varepsilon(t)$, where each coefficient b_i (for $i = 0, 1, 2, \ldots, M$) is a constant and does not vary with time within the temporal period examined, which measures stationary influence of X_i on Y; M is the number of predictors and $\varepsilon(t)$ is the error term. In real climate system, however, the relationship between Y and X_i is often nonstationary. For instance, Xie et al. (2010) showed that the influence of El Niño on the subtropical northwest Pacific climate has significantly

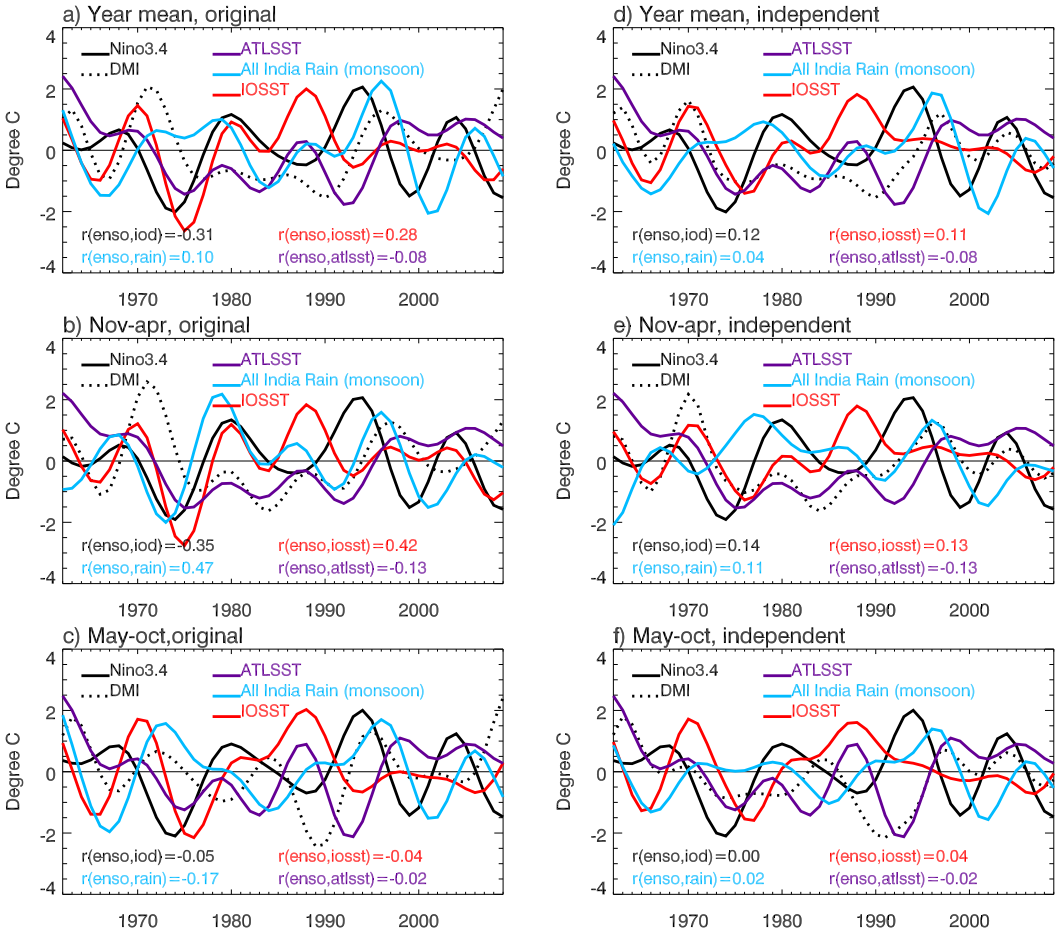

FIG. 3. (a) The 8-yr low-pass-filtered climate indices based on the annual mean Niño-3.4 index (black solid); Indian Ocean DMI (black dashed); Indian Ocean SST index averaged over 15°S–15°N, 50°–95°E (red); Atlantic SST index averaged over 30°S–60°N, 70°W–20°E (purple); and annual total of all Indian monsoon rainfall (mm) index (cyan). (b) As in (a), but based on winter (November–April) data; (c) as in (a), but based on summer (May–October) data. The 1960–2011 linear trend is removed and each index is normalized by its standard deviation.(d)–(f) As in (a)–(c), but removing the ENSO effect on DMI, Indian Ocean SST and monsoon using Bayesian DLM. The effects of summer monsoon rainfall on DMI and Atlantic SST on the summer monsoon are also removed. Consequently, the predictors shown in (d)–(f) are independent of each other.

increased after the 1970s; Annamalai et al. (2005) demonstrated that the ENSO–IOD relation has an apparent change after 1976; Kumar et al. (1999) documented that the ENSO–Indian summer monsoon relation has broken down during recent decades (also see Ashok et al. 2001); and Krishnaswamy et al. (2015) argued that the IOD effect on Indian summer monsoon has strengthened in recent decades compared to ENSO.

The Bayesian DLM allows coefficients b_i to vary with time, which overcomes the limitation of constant coefficients of the SLM and thus measures dynamical (time evolving) impacts of X_i on Y. The DLM consists of two equations: an "observation equation" analogous to the SLM [see Eq. (1) below] and a "state equation" that controls the dynamical evolution of coefficients b_i [represented by Eq. (2)]:

$$Y(t) = b_0(t) + b_1(t)X_1(t) + \cdots + b_M(t)X_M(t) + \varepsilon(t), \quad \text{where} \quad \varepsilon(t) \sim N[0, V(t)], \quad \text{and} \tag{1}$$

$$b_i(t) = b_i(t-1) + w_i(t), \quad \text{where} \quad w_i(t) \sim N[0, W_i(t)]. \tag{2}$$

The state Eq. (2) means that the predictive distribution of b_i at each time step t (i.e., posterior) is updated based on its previous step $t-1$ distribution (i.e., prior) and the probability of observations Y conditional on b_i at time t

(i.e., the likelihood) using Bayes theorem (Petris et al. 2009). Coefficient b_i is obtained by applying Kalman filtering and smoothing, with the regression coefficient of SLM as its initial guess.

In Eqs. (1) and (2), the $b_0(t)$ term represents a time-varying level or intercept whose variability is unexplained by the independent predictors X_i, while the b_i terms represent the nonstationary influence of X_i on Y; $\varepsilon(t)$ and $w_i(t)$ are independent white noises or errors, distributed normally with a mean of 0 and variances of $V(t)$ and $W_i(t)$. In recent studies of Krishnaswamy et al. (2015) and Yanto et al. (2016), V was obtained from the residual error variance of the SLM, and W_i was specified a priori by setting $W_i/V = 0.1$, and thus both are constant in time and W is independent of i. In this paper, we calculated $W_i(t)$ and $V(t)$ using the maximum likelihood estimation (MLE) method (Petris et al. 2009) recommended by G. Petris (2016, personal communication), which allows W_i and V to vary with time (also see Osthus 2015). The DLM results using the MLE method are almost identical to those using specified V and W described above. In this paper, all the DLM results shown are from the specified V and W. For more details of the Bayesian DLM, please see Petris et al. (2009), Petris (2010), and R Development Core Team (2016).

d. Partial Bayesian DLM approach

Since the decadal ENSO and IOD indices are moderately correlated (Figs. 3a–c) and yet the DLM requires the predictors to be independent, we apply the Bayesian DLM to the DMI using ENSO index as the predictor, and then remove the ENSO-associated part from the original DMI. Since the intensity of Indian summer monsoon can also affect the IOD strength on interannual time scales (e.g., Krishnan and Swapna 2009) and their decadal variability is moderately correlated (not shown), we also remove the monsoon effect. This procedure is referred to as partial DLM, and the DMI with ENSO and monsoon effects removed is independent of ENSO and monsoon (Figs. 3d–f). Using ENSO and IOD as predictors, Eq. (1) becomes

$$Y(t) = b_0(t) + b_1(t)\mathrm{ENSO}(t) + b_2(t)\mathrm{IOD}(t) + \varepsilon(t), \quad (3)$$

where $Y(t)$ represents the Indian Ocean WC, Pacific WC, or warm-pool convection.

Similarly, we remove ENSO's effect on Indian summer monsoon and Indian Ocean SST indices (e.g., Klein et al. 1999; Du et al. 2009), and the Atlantic SST effect on the monsoon index. These indices are shown in Figs. 3d–f. Then, we apply the Bayesian DLM to the residual Y', with $Y' = Y(t) - b_1(t)\mathrm{ENSO}(t) - b_2(t)\mathrm{IOD}(t)$, using the monsoon index as the predictor. Subsequently, we apply the DLM to $Y' - Y(\mathrm{monsoon})$, using Indian Ocean SST and Atlantic SST indices as predictors. We separately examine the monsoon effect versus Indian and Atlantic Ocean SST, to avoid overfitting with the limited data record for the SLM and DLM (e.g., Babyak 2004).

The objective of partial DLM is to sequentially remove the influence of the preceding predictors so that each predictor in the DLM is independent. The consequence of this procedure for attribution, however, is that if two predictors are correlated, then the shared influence on the predictand is attributed to the predictor that is added to the model first (e.g., ENSO, IOD, monsoon, and tropical Indian and Atlantic Ocean SST). The Bayesian DLM approach is rather new, and it has been recently applied to climate studies to understand the nonstationary effects of ENSO and IOD on interannual variability of the Indian summer monsoon (e.g., Krishnaswamy et al. 2015) and Indonesian rainfall (Yanto et al. 2016).

3. Decadal variability of warm-pool convection and WCs and their covariability

In this section, we first document decadal variability of the warm-pool convection and Indo-Pacific WCs, and their seasonality and covariability (section 3a). Then, we investigate the decadal covariability between the Indian and Pacific Ocean WCs (section 3b).

a. Variability of warm-pool convection and WCs

To illustrate the decadal variability of warm-pool convection, we obtain the time series of 8-yr low-pass-filtered ICOADS cloudiness and CRU precipitation over land averaged over the warm-pool region from 1960 to 2010, together with the OLR and GPCP precipitation from 1983 to 2010 (Fig. 2c). Since the warm-pool OLR is a proxy of deep convection that drives the WCs, whereas cloudiness may contain cloud types (e.g., cirrus cloud) that are not associated with convection, we compare OLR and cloudiness (CLD) for their overlapping period. Their correlation is $r(\mathrm{CLD}, -\mathrm{OLR}) = 0.68$ below 90% significance, which is somewhat lower than the CRU and $-$OLR correlation of 0.75 (>90% significance). The CRU precipitation, however, is only available over land. To understand how well it represents precipitation over the entire warm-pool region, we compare the CRU data with GPCP precipitation, which is available over both land and ocean. The two agree reasonably well, with a correlation coefficient of 0.91 (>90%). The significance test has considered the reduced degrees of freedom due to filtering (Livezey and

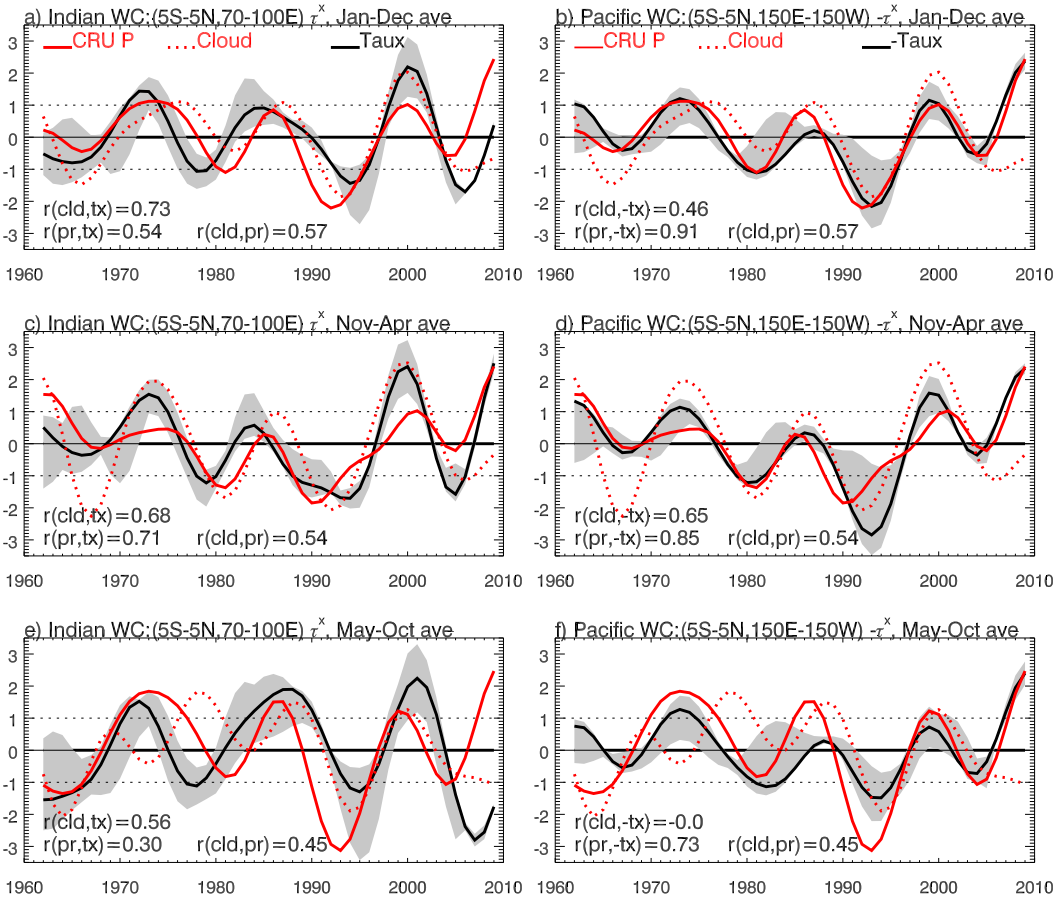

FIG. 4. (a) Time series of 8-yr low-pass-filtered CRU precipitation over land averaged over the land stations within the warm pool (black box in Fig. 2) from 1962 to 2009 (red solid curve), together with 8-yr low-pass-filtered ICOADS cloudiness averaged over the warm pool (red dotted curve) and Indian Ocean WC strength (black solid curve), represented by 8-yr low-pass-filtered τ^x averaged over 5°S–5°N, 70°–100°E, using annual mean data. (b) As in (a), but using November–April mean data. (c) As in (a), but using May–October mean data. (d)–(f) As in (a)–(c), but for the Pacific WC strength (black solid), which is represented by $-\tau^x$ averaged over 5°S–5°N, 150°E–150°W. The negative sign ensures that a surface easterly wind anomaly corresponds to an intensified Pacific WC. For each panel, the wind curve (black) shows the averaged NCEP–NCAR and JRA-55 data, the two datasets that have longer records. The gray-shaded area shows the range of winds from NCEP–NCAR, WASWind, JRA-55, and ORAS3 data for 1962–2005 when all products are available, and from NCEP–NCAR and JRA-55 for 2006–09. Using the average of all four winds for 1962–2005 yields similar results, but with lower correlation with warm-pool CRU precipitation and ICOADS cloudiness. The first and last four years are removed to exclude the filter's end point effect. Each curve is normalized by the standard deviation of its annual mean data.

Chen 1983). In addition, compared to the cloudiness, CRU precipitation has higher correlation with the Pacific WC for all seasons and somewhat higher correlation with the Indian Ocean WC during winter (Fig. 4). For these reasons, we use the CRU precipitation to represent decadal variability of warm-pool convection hereafter, even though the interannual variability (with monthly climatology removed) of warm-pool cloudiness and −OLR is more correlated (r = 0.9) than that of CRU and −OLR (r = 0.70) based on the raw monthly data from 1983 to 2009, because this paper focuses on decadal variability.

Note that quantitative differences exist between CRU and GPCP data. Part of the difference may result from the fact that CRU data are available only over land areas of the warm pool. Note also that the summertime correlation between cloudiness and Indian Ocean WC (defined below) is 0.56, which is higher than the CRU–Indian Ocean WC correlation of 0.30 (Fig. 4e). This is likely due to the cloudiness including the ocean areas of the warm pool on the Indian Ocean side, which is related to the Indian Ocean WC for the May–October season, when the IOD develops and becomes mature.

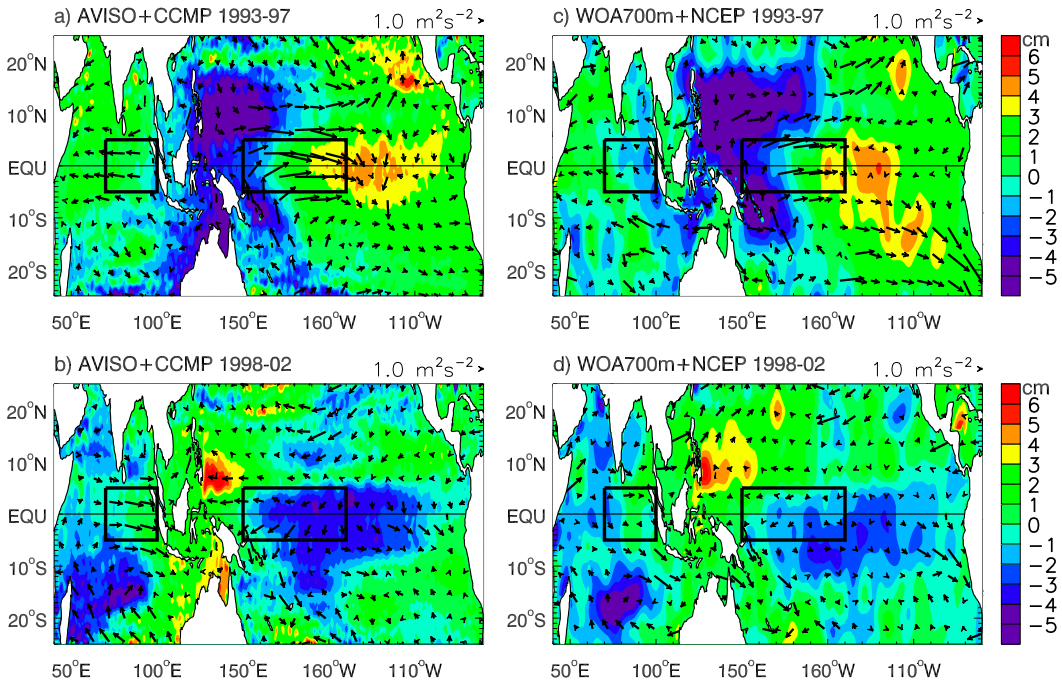

FIG. 5. SSHA (with global and climatological means removed) based on monthly AVISO satellite data (color shading) and monthly CCMP pseudo wind stress (arrows) averaged for (a) 1993–97 and (b) 1998–2002, the periods when the WC anomalies are negative (weaken) and positive (strengthen), respectively, according to Fig. 4. (c),(d) As in (a),(b), but for the upper-700-m thermosteric sea level from *WOA13* data and NCEP–NCAR reanalysis wind. Using Ishii and Kimoto (2009) upper-700-m thermosteric sea level and JRA-55 wind yields similar results. No low-pass filter is applied for this figure. The black boxes represent the eastern Indian Ocean (5°S–5°N, 70°–100°E) and western Pacific (5°S–5°N, 150°E–150°W), which are used to form time series of zonal surface winds that represent WCs' strength in Fig. 4 and later figures.

Decadal variations of warm-pool convection are positively correlated with the Indian and Pacific Ocean WCs overall for the 1962–2009 period, with enhanced (weakened) convection being often, even though not always, associated with anomalous surface wind convergence (divergence) and thus enhanced (weakened) WCs over the two oceans (Figs. 4a,b). In this paper, the Indian Ocean WC is defined as surface τ^x averaged over 5°S–5°N, 70°–100°E, with the latitudinal range adopted by Meehl et al. (2003). The Pacific WC is defined as zonal wind stress averaged over 5°S–5°N, 150°E–150°W multiplied by −1 (i.e., $-\tau^x$), a definition ensures that an easterly wind anomaly corresponds to a strengthened Pacific WC. Indeed, systematic changes of surface winds occur in the two regions during the positive and negative periods of warm-pool convection anomalies (boxed regions in Fig. 5).

The covariability, however, exhibits evident seasonality particularly for the Indian Ocean WC. During the November–April Indonesian wet but Indian monsoon dry season of winter, decadal variability of the warm-pool convection and WCs is strongly correlated, with correlation coefficient of 0.85 (>95% significance) for convection–Pacific WC and 0.71 (>95%) for convection–Indian Ocean WC (Figs. 4c,d). In contrast, during the May–October Indonesian dry and Indian summer monsoon wet season (Figs. 4e,f), variability of the warm-pool convection is not significantly correlated with the Indian Ocean WC (r = 0.3), and its correlation with the Pacific WC (r = 0.73; >95%) is also lower than the winter value. Therefore, the moderate covariability for convection and Indian Ocean WC using annual mean data (r = 0.54; <90% significance) results primarily from their wintertime covariability, and the high covariability for convection and Pacific WC in the annual mean (r = 0.91; >95%) arises from the consistently high correlations during both seasons, even though the covariability decreases somewhat in summer.

The seasonality of convection–WC covariability for both oceans is robust to cross-dataset differences using WASWind, NCEP–NCAR, JRA-55, and ORAS3 winds to represent the WCs, even though there are quantitative differences among datasets (figure not shown). In all of our figures, time series of the WCs are represented by the averaged NCEP–NCAR and JRA-55 winds, which have longer records of 1962–2009 after 8-yr low-pass

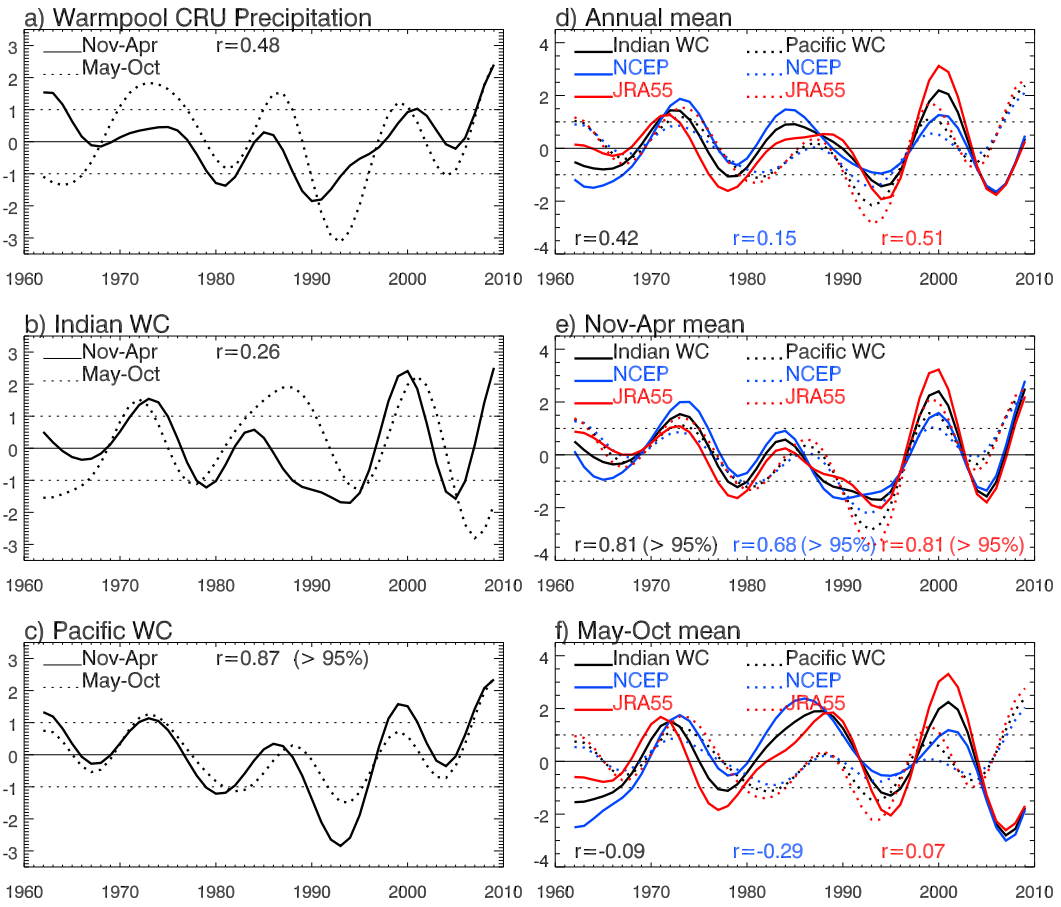

FIG. 6. (a) Time series of 8-yr low-pass-filtered CRU precipitation averaged in the warm pool for winter (November–April; solid) and summer (May–October; dotted) season from 1962 to 2009. (b),(c) As in (a), but for the time series of Indian and Pacific Ocean WC, respectively. (d) Time series of 8-yr low-pass-filtered Indian (solid black) and Pacific (dashed black) Ocean WCs from 1962 to 2009 based on annual mean, averaged NCEP–NCAR and JRA-55 data; as a comparison, the WCs using NCEP–NCAR (blue) and JRA-55 (red) individual datasets are also shown. (e),(f) As in (d), but using November–April and May–October mean data, respectively. Each curve is normalized by its standard deviation. Correlations above 95% significance are shown in parentheses after the correlation value.

filtering. Averaged winds from all four-wind products for 1962–2005 are also tested, and we obtained similar results but with somewhat lower correlation with warm-pool convection.

Given that the covariability reduces considerably for convection with the Indian Ocean WC but only weakly with the Pacific WC during summer, the evident reduction over the Indian Ocean likely results from strong seasonality of the Indian Ocean WC. To confirm this point, we compare the winter and summer evolutions of the warm-pool convection, Indian Ocean WC, and Pacific WC, respectively (Figs. 6a–c). Indeed, decadal variability of the Indian Ocean WC shows the strongest seasonal variability, with winter–summer correlation being only $r = 0.26$ from 1962 to 2009. The seasonality of warm-pool convection is moderate ($r = 0.48$; <95%), compared to the lesser seasonality of the Pacific WC ($r = 0.87$; >95%).

b. *Covariability between the Indian and Pacific Ocean WCs*

Do the Indian and Pacific Ocean WCs covary, and does their covariability also exhibit seasonality? To answer this question, we compare the Indian and Pacific Ocean WCs for each season (Figs. 6d–f). During northern winter, decadal variability of the Indian Ocean WC covaries well with the Pacific WC, with correlation being 0.81 from 1962 to 2009 for the averaged NCEP–NCAR and JRA-55 winds and JRA-55 winds alone, and being 0.68 for NCEP–NCAR winds alone (Fig. 6e). By contrast, during northern summer their decadal variability is independent and essentially uncorrelated

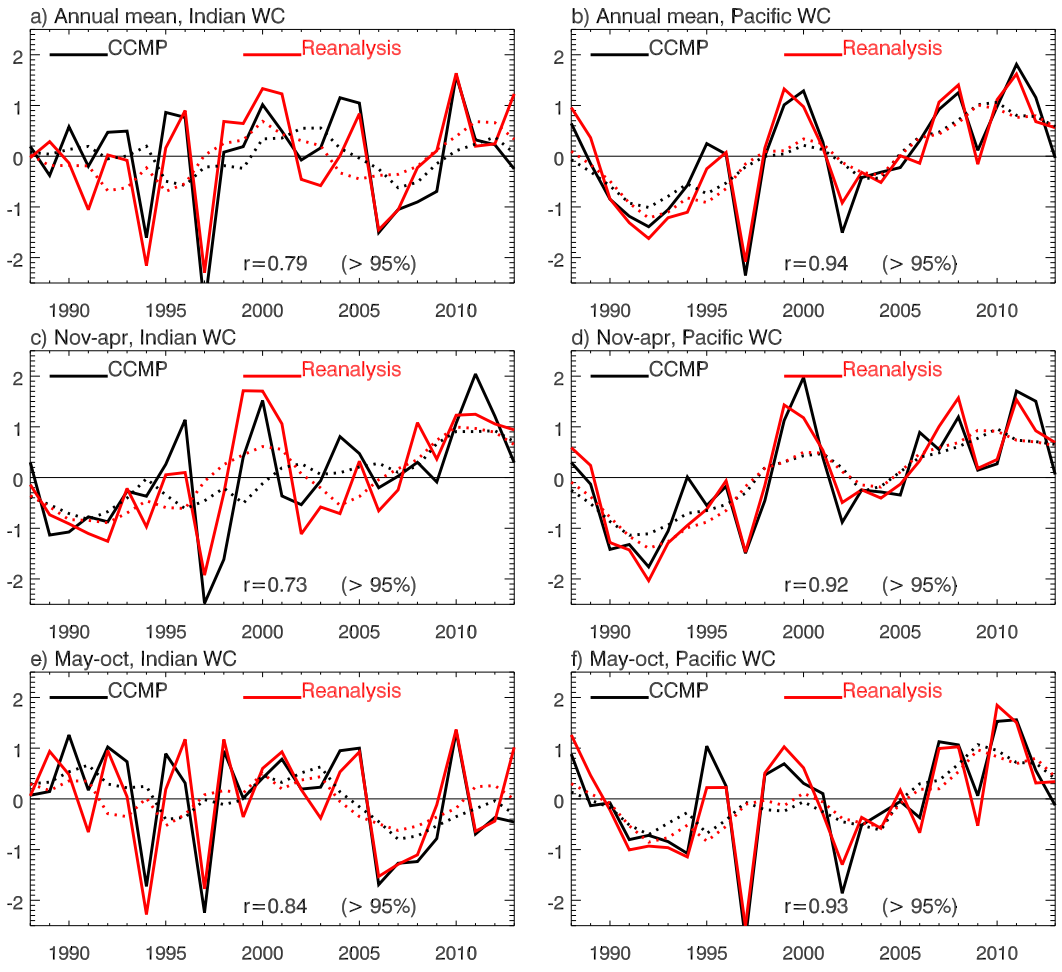

FIG. 7. Comparison of the (a) Indian and (b) Pacific Ocean WC defined in section 3a of the text and in the caption of Fig. 4 using CCMP satellite winds (black curve) and averaged NCEP–NCAR and JRA-55 data (red curve) for their overlapping period of 1988–2013 based on annual mean data. (c),(d) As in (a),(b), but using November–April mean data. (e),(f) As in (a),(b), but for May–October mean data. Each curve is normalized using its standard deviation. Dotted curves are their corresponding 5-yr running means.

(Fig. 6f), which explains the relatively low correlation in the annual mean ($r = 0.42$ for averaged NCEP–NCAR and JRA-55 winds; Fig. 6d) compared to winter. This is related to the geography of the Indo-Pacific region, whereby the convective maximum during winter is near the equator over the Maritime Continent, whereas during summer it lies well north of the equator over South Asia (Meehl 1987). Thus, zonal features (e.g., the WCs) are likely to have stronger connections in winter when the seasonal convection over the Indo-Pacific is closer to the equator. In summer, however, off-equatorial convection associated with Indian monsoon can have strong influence on the Indian Ocean WC and therefore reduce its covariability with the Pacific WC (see section 4b below).

To further confirm the decadal variability of the WCs detected by reanalysis winds, we compare them with the CCMP satellite winds for their overlapping period of 1988–2013. The reanalysis winds agree well with the CCMP winds (Fig. 7), particularly for the Pacific WC where their correlations are above 0.92 for all seasons (Figs. 7b,d,f). The discrepancies are larger for the Indian Ocean WC, but the agreement remains reasonably strong, with correlations ranging from 0.73 to 0.84 (Figs. 7a,c,e), which correspond to approximately 53%–69% variance. Consistent with the surface wind diverging from (converging into) the warm-pool region associated with the weakening (enhancing) Indian and Pacific Ocean WCs, sea level falls (rises) in the equatorial eastern Indian and western Pacific Oceans, as shown by both the satellite-observed SSHA and in situ based thermosteric sea level (Fig. 5). The spatial patterns of satellite-observed SSHA and surface winds are reasonably reproduced by the *WOA13* upper-700-m thermosteric sea

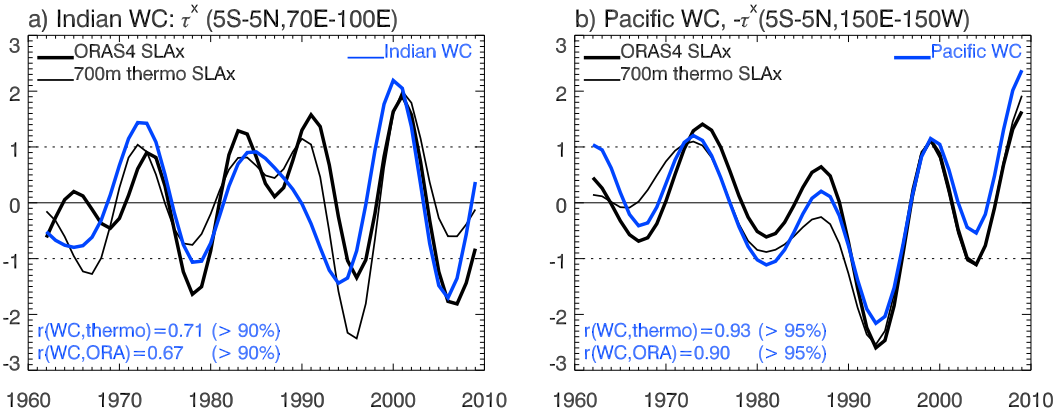

FIG. 8. (a) Time series of 8-yr low-pass-filtered Indian Ocean WC (zonal wind stress anomaly averaged for 5°S–5°N, 70°–100°E) from averaged NCEP–NCAR and JRA-55 data (blue curve), together with zonal gradients of ORAS4 total SLA (thick black) and 700-m thermosteric sea level from averaged *WOA13* and Ishii and Kimoto (2009) data (thin black). Each curve is normalized by its standard deviation for the 1962–2009 period. (b) As in (a), but for the Pacific WC (negative zonal wind stress anomaly averaged for 5°S–5°N, 150°E–150°W) and zonal SLA gradient. The SLA gradients are defined in section 3b.

level and reanalysis winds, even though there are some quantitative differences. The Ishii and Kimoto (2009) thermosteric sea level shows similar results, albeit with some quantitative disparities (not shown).

Before the satellite era, decadal variations of the Indian and Pacific Ocean WCs shown by the reanalysis winds are also supported by the observed upper-700-m thermosteric sea level and ORAS4 reanalysis sea level, which show overall consistency over the two oceans (Fig. 8). The correlation coefficients between the WCs and zonal sea level gradient [*WOA13* and Ishii and Kimoto (2009) average] are 0.71 (>90%) over the Indian Ocean and 0.93 (>95%) over the Pacific for the 1962–2009 period. For the Indian Ocean, the sea level anomaly (SLA) gradient is calculated by SLA averaged for 5°S–5°N, 80°–95°E subtracting that for 5°S–5°N, 65°–80°E, which are approximately the east and west portions of the Indian Ocean WC region (Figs. 5b and 5d, respectively) and thus represent the WC effect on sea level gradient. For the Pacific, it is measured by SLA averaged for 5°S–5°N, 130°E–180° subtracting that for 5°S–5°N, 180°–130°W, which are approximately the west and east portions of the Pacific WC (Fig. 5) defined by $-\tau^x$. Since the thermosteric sea level data are independent datasets from the reanalysis winds, their good agreements (see section 2a for scientific justification) increase our confidence in the decadal variations of the Indian–Pacific WCs detected by reanalysis winds since the 1960s.

4. Effects of decadal variability of climate modes and other climate indices

What are the major causes for the decadal variability of the Indian and Pacific Ocean WCs and warm-pool convection? Given that ENSO and IOD are the two dominant climate modes over the Indo-Pacific basin and they are closely related to the WCs and warm-pool convection (section 1), in this section we first examine the effects of their decadal variability using the Bayesian DLM (section 4a). Then in section 4b we assess the associations of WC variability with other climate indices: decadal variability of the Indian summer monsoon convection, Indian Ocean basinwide SSTA, and Atlantic SSTA defined in section 2b (Fig. 3).

a. *Variability of the WCs associated with decadal variability of ENSO and IOD*

For the Pacific WC, the Bayesian DLM solutions agree remarkably well with the observations for both the November–April winter season and May–October summer season (thick solid and dotted curves of Figs. 9a,d), with model–data correlation of $r = 0.98$ and standard deviation (STD) ratio of $\mathrm{STD}_{\mathrm{model}}/\mathrm{STD}_{\mathrm{obs}} = 0.95$ for both seasons from 1962 to 2009. The conventional SLM also yields highly consistent results, with the model–data correlation and STD ratio both being 0.89 for winter and 0.92 for summer (gray curves of Figs. 9a,d). Decadal ENSO is the predominant cause for the WC variability, with decadal IOD playing a minor role (red and blue curves of Figs. 9b,e).

Because of the dominant role played by ENSO, we explore its dynamical impacts by analyzing its DLM coefficient and compare it with the SLM coefficient (Figs. 9c,f). During winter, the effect of ENSO decadal variability—as shown by DLM coefficient b_1 (red curve of Fig. 9c)—has significant variations, being weaker during the 1970s with a minimum magnitude of

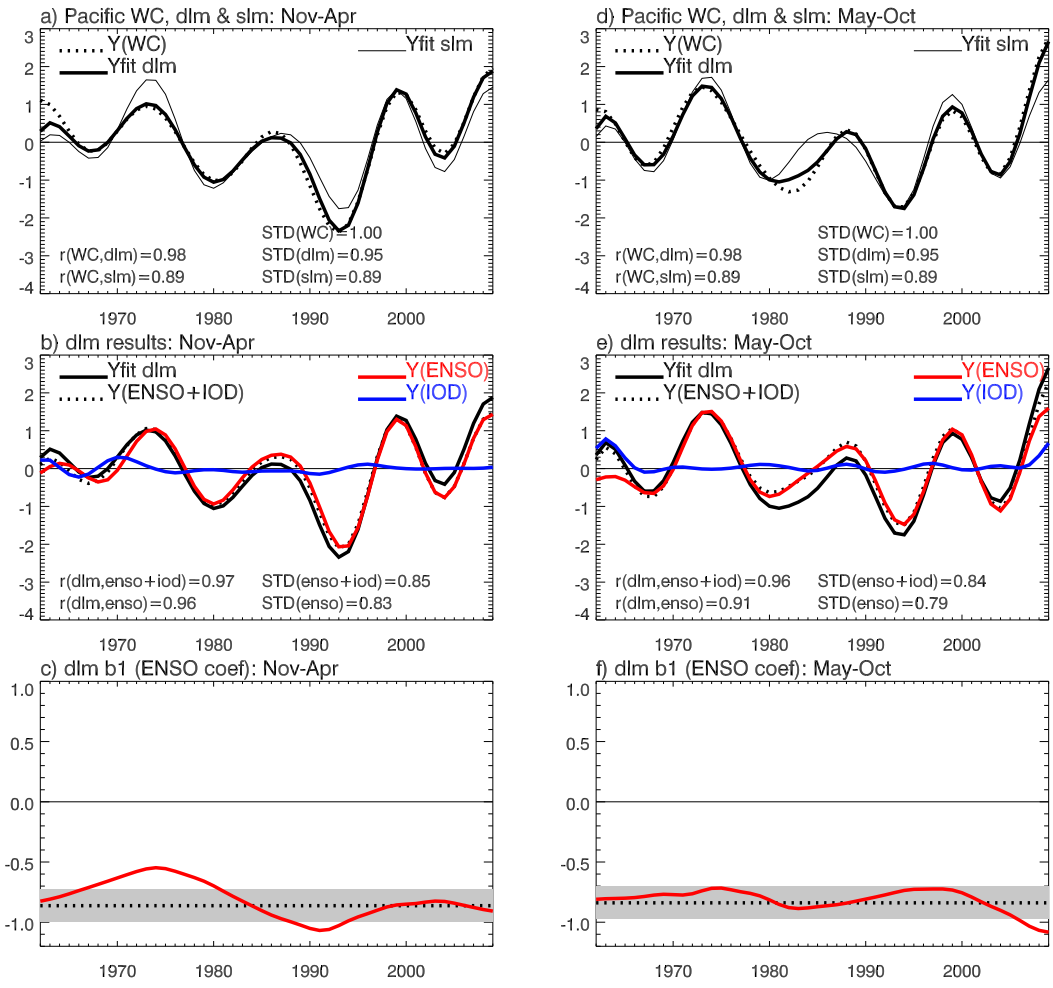

FIG. 9. (a) Time series of 8-yr low-pass-filtered normalized Pacific WC for November–April mean from averaged NCEP–NCAR and JRA-55 data for the 1962–2009 period [Y(WC); dotted curve], its Bayesian DLM simulation using ENSO and IOD indices as predictors (''Yfit dlm''; black solid curve), which is $b_0(t) + b_1(t)\text{ENSO}(t) + b_2(t)\text{IOD}(t)$ in Eq. (3), and result from conventional static linear model ("Yfit slm"; thin gray curve). The STD for each curve and correlations between them are also shown. (b) Yfit dlm duplicates the solid black curve of (a), Y(ENSO) is ENSO-associated WC (red) and is the $b_1(t)$ENSO(t) term, Y(IOD) is IOD-associated WC (blue) and is the $b_2(t)$IOD(t) term, and Y(ENSO + IOD) is their sum. (c) Bayesian DLM coefficient for ENSO (b_1, red curve) determined by Eq. (2); as a comparison, the corresponding static linear model regression coefficient is plotted as dotted line with 95% confidence interval shown by gray shading. (d)–(f) As in (a)–(c) respectively, but using May–October mean data.

$b_1 \approx -0.5$, and stronger in the early 1990s with a maximum magnitude of $b_1 \approx -1.0$, and both exceeding the 95% confidence interval of the SLM coefficient (dotted line of Fig. 9c). The increased b_1 magnitude indicates that for the same strength of ENSO index, its impact on the WC is larger. Understanding the physical causes for this changing impact is beyond the scope of this paper, but it is an important theme of our future research. During summer, the influence of ENSO decadal variability is rather persistent, with b_1 being within the 95% confidence interval of the SLM coefficient for most of the time, except for the late 2000s when the magnitude of b_1 becoming large (Fig. 9f). The negative b_1 demonstrates that El Niño–like (La Niña–like) decadal variability weakens (enhances) surface easterlies and thus weakens (intensifies) the Pacific WC.

Because of the vital influence of ENSO decadal variability, the total effect of ENSO and IOD explains most of the observed and simulated variability (Figs. 9a,b and 9d,e, respectively), and the residual between the observed and (ENSO and IOD) simulated variability is small. Therefore, the influences of other climate indices

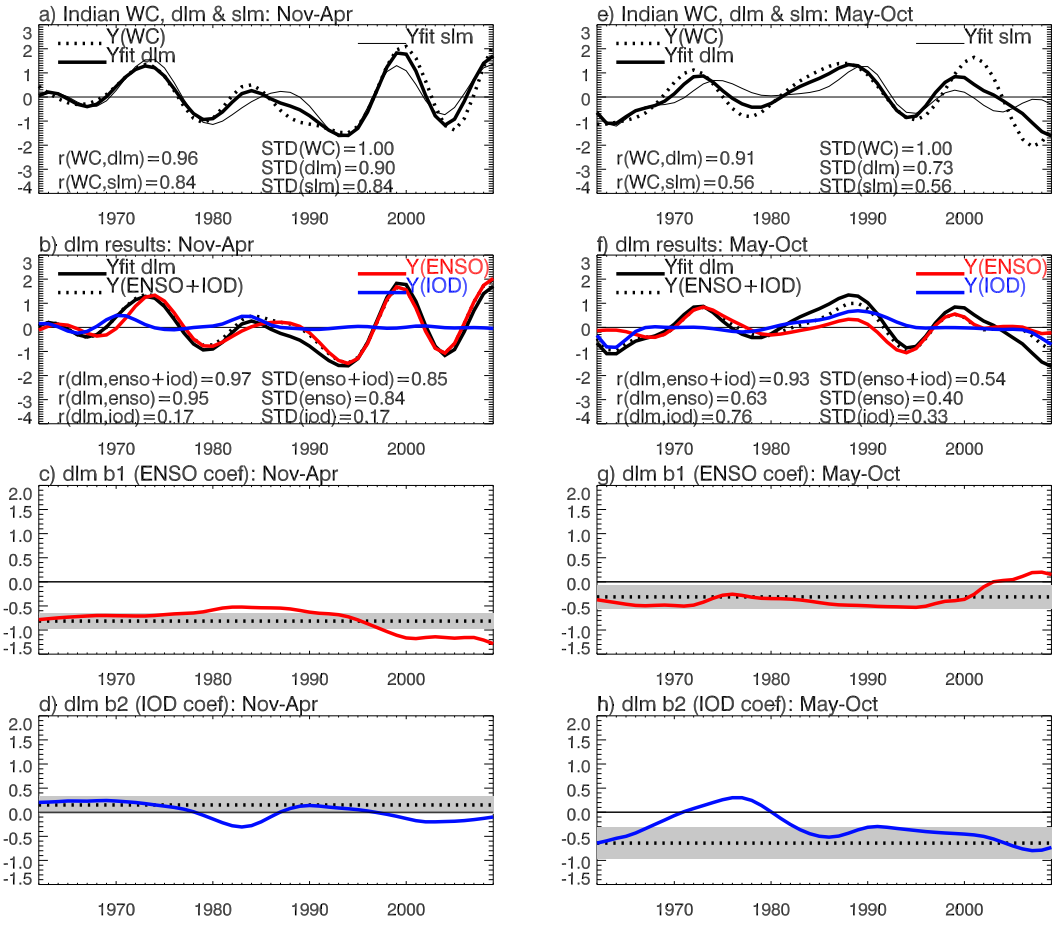

FIG. 10. As in Fig. 9, but for the time series of 8-yr low-pass-filtered normalized Indian Ocean WC. (d),(h) Decadal IOD coefficients (b_2, blue curve) are also shown since the IOD effect is larger than that for the Pacific WC for the May–October season.

(i.e., Indian monsoon and Atlantic and Indian Ocean SST) are weak using the partial DLM approach described in section 2d and thus are not shown.

Compared to the Pacific, causes for the decadal variability of the Indian Ocean WC are more complex, particularly during the May–October summer season. During winter, the DLM is able to reasonably simulate the observed WC (thick solid and dotted curves of Fig. 10a), and decadal ENSO still dominates decadal IOD in determining the WC variability (red and blue curves of Fig. 10b). The effect of ENSO decadal variability is relatively weak during the 1980s ($b_1 \approx -0.5$) but strong after 2000 ($b_1 \leq -1.0$), exceeding the 95% confidence interval of the SLM coefficient (red curve and dotted line of Fig. 10c). This time-varying effect of ENSO cannot be represented by the SLM, which explains the deteriorating fit of the SLM (thin gray curve of Fig. 10a) compared to the DLM. These results indicate that El Niño–like (La Niña–like) decadal variability weakens (strengthens) the equatorial westerlies over the eastern Indian Ocean and thus weakens (enhances) the Indian Ocean WC. The effect of IOD decadal variability remains weak compared to ENSO (blue and red curves of Figs. 10b,f). Its DLM coefficient b_2 is close to 0 during most of the time except for the early 1980s and after 2000, when b_2 is weakly negative and exceeds the 95% confidence interval of the SLM coefficient. The negative b_2 suggests that positive IOD-like decadal variability weakens the Indian Ocean WC, analogous to their relationship on interannual time scale (e.g., Saji et al. 1999; Meehl and Arblaster 2002; Meehl et al. 2003). The dominant effect of ENSO decadal variability on both the Pacific WC and wintertime Indian Ocean WC explains their observed high covariability for the November–April season (section 3b).

During summer, the Bayesian DLM solution agrees reasonably with the observed Indian Ocean WC, with model–data correlation of 0.91 and STD ratio of 0.73,

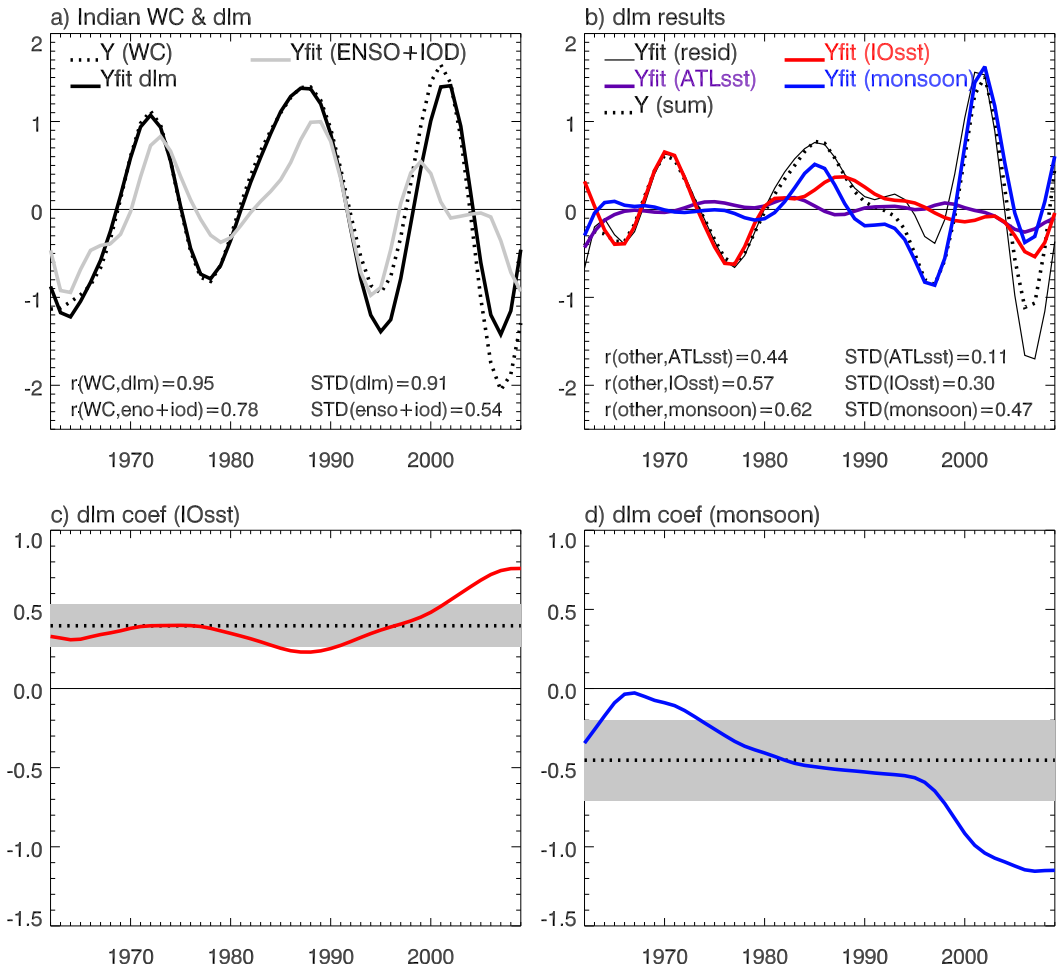

FIG. 11. (a) Observed time series of 8-yr low-pass-filtered Indian Ocean WC Y(WC) (dotted curve), DLM results including effects of ENSO, IOD, monsoon, and Indian and Atlantic Ocean SST Yfit dlm (thick solid black curve), together with ENSO plus IOD effect Yfit(ENSO + IOD) (gray). (b) DLM simulation of the residual Indian Ocean WC, Y(WC) − Y(ENSO + IOD), denoted by "Yfit (resid)" (thin black curve), together with the part associated with Atlantic SST (purple), Indian Ocean SST (red), Indian summer monsoon (blue), and their sum (dotted). (c) DLM coefficient for Indian Ocean SST effect (red) and the static linear model regression coefficient (dotted line) with 95% confidence interval (gray shading). (d) As in (c), but for DLM coefficient of Indian summer monsoon (blue curve).

compared to the correlation and STD ratio of 0.56 from the SLM (Fig. 11e). The total effect of decadal ENSO and IOD, however, only explains 54% of the observed STD ($STD_{ENSO+IOD}/STD_{obs}$ = 0.54; Fig. 10f), suggesting that a large fraction of summertime WC variability cannot be explained by ENSO and IOD decadal variability. The STD ratio of decadal ENSO contribution is 0.40 and its correlation with the total DLM solution is 0.63, while those for the decadal IOD are 0.33 and 0.76, suggesting that their overall effects are comparable (also see Figs. 10g,h). The overall negative b_1 and b_2 are consistent with the effects of decadal ENSO and IOD for winter (see above). During the late 1970s, however, b_2 is weakly positive, which opposes the relationship between the Indian Ocean WC and the IOD decadal variability discussed above. This is because of the large effect of basin-mean Indian Ocean SSTA, as explained next in section 4b.

b. *Variability of the WCs associated with the Indian summer monsoon and Indian and Atlantic Ocean SST*

What are the causes for the large fraction of the Indian Ocean WC variability that is unexplained by decadal ENSO and IOD during summer (cf. the black dotted and gray curves of Fig. 11a)? To answer this question, we use the partial Bayesian DLM approach to assess the effects of Indian summer monsoon convection, Atlantic

SST, and Indian Ocean SST using their indices as predictors (sections 2b–d; Fig. 3). While the effect of Atlantic SST is small overall (purple curve of Fig. 11b), both the Indian summer monsoon and Indian Ocean SST variability contribute significantly to the variability of the Indian Ocean WC (blue and red curves of Fig. 11b). Whereas the Indian Ocean SST dominates the monsoon effect before the late 1980s, the effect of the monsoon dominates afterward. Indeed, the monsoon effect is the major cause for the large-amplitude decadal variability since the late 1990s and it also dominates the decadal ENSO and IOD effect for this period (cf. Figs. 11a and 11b).

Recall that the ENSO impact is removed from the monsoon index in our Bayesian DLM. Thus, variations of monsoon index shown in Fig. 3f are independent of ENSO. Indeed, the monsoon index prior to removing ENSO shows an out-of-phase relation with ENSO index approximately before the 1990s, as documented by existing studies (e.g., Torrence and Webster 1999). This relationship, however, breaks down approximately after the 1990s (black solid and blue curves of Fig. 3c), suggesting that decadal variability of Indian summer monsoon convection during recent decades is induced by factors other than ENSO. The increased importance of the Indian summer monsoon since the late 1990s is clearly seen in the DLM coefficient, which has exceeded the 95% confidence interval of the SLM coefficient since about 1998 (Fig. 11d). The DLM results with ENSO signals retained in both the monsoon index and the WC show a similar increased impact of monsoon, even though its effect is larger during the 1960s–1970s (figure not shown).

During the 1960s–1970s, the effect of Indian Ocean SST is strong, while the monsoon influence is weak (Fig. 11b), even though the DLM coefficient of Indian Ocean SST is close to the SLM coefficient (Fig. 11c). This is because the amplitude of Indian Ocean SST index is large (red curve of Fig. 3), and the ''effect'' is measured by the product of the index and DLM coefficient. The positive DLM coefficient (Fig. 11c) suggests that a cold SSTA averaged over the tropical Indian Ocean during the late 1970s (red curve of Fig. 3f) weakens the Indian Ocean WC, even though the eastern basin is somewhat warmer than the western basin, which corresponds to the negative IOD-like situation (dotted curve of Fig. 3f). The weakened WC due to the strong influence of negative Indian Ocean SSTA exceeds the increased WC due to the negative IOD-like variability during the 1970s, which explains the weak positive DLM coefficient of decadal IOD shown in Fig. 10h, because a weakened Indian Ocean WC is associated with a negative IOD index for this period of time. Note that, similar to the SLM, the DLM in fact assesses the relationship between the predictor and predictand, rather than the causality.

The negative coefficient for Indian summer monsoon and positive coefficient for Indian Ocean SST indicate that a weak monsoon and warm Indian Ocean favor an intensified Indian Ocean WC (see section 5 for discussion of possible mechanisms). The complex causes for the Indian WC variability during summer (i.e., decadal ENSO, IOD, Indian Ocean SST, and Indian summer monsoon) are the major reason for its incoherent variability with the Pacific WC, which is determined almost solely by ENSO decadal variability.

c. *Variability of warm-pool convection associated with climate indices*

Using ENSO and IOD as predictors, the Bayesian DLM also yields reasonable simulations for warm-pool convection particularly during the May–October Indonesian dry season, when data–model correlation is 0.98 and STD ratio is 0.93 from 1962 to 2009 (thick black solid and dotted curves of Fig. 12d). For the November–April wet season, the data–model correlation is 0.94 and STD ratio is 0.81 (Fig. 12a), which are somewhat lower than those of summer. The SLM is less accurate for both seasons, especially for the wet season when data–model correlation and STD ratio are both 0.67 (thin gray curve of Fig. 12a). The total effect of ENSO and IOD decadal variability explains most of the observed variability of convection, with STD ratio of 0.89 in summer and 0.61 in winter. The ENSO decadal variability plays a dominant role compared to IOD for both seasons (Figs. 12b,e). The caveat for the weak IOD effect is that the CRU precipitation, which is used to represent warm-pool convection, is only available over lands, whereas the IOD may have large influence on convection and precipitation over the ocean area of the eastern Indian Ocean. This speculation is supported by the larger effect of the IOD on cloudiness, which has values over both lands and ocean (not shown), and the comparable effect of the IOD and ENSO on the Indian Ocean WC (Fig. 10f).

Can the residual of warm-pool convection, $Y - Y(\text{ENSO} + \text{IOD})$, be explained by other climate indices particularly in winter? To answer this question, we applied the partial DLM to the residual using the Indian summer monsoon, tropical Indian Ocean SST and Atlantic SST indices as predictors, but neither the individual predictors nor their sum can simulate the residual convection (not shown). This result indicates that the relationship between the warm-pool convection/precipitation and SSTA (e.g., ENSO and IOD indices) during the wet season, when precipitation is strong, may

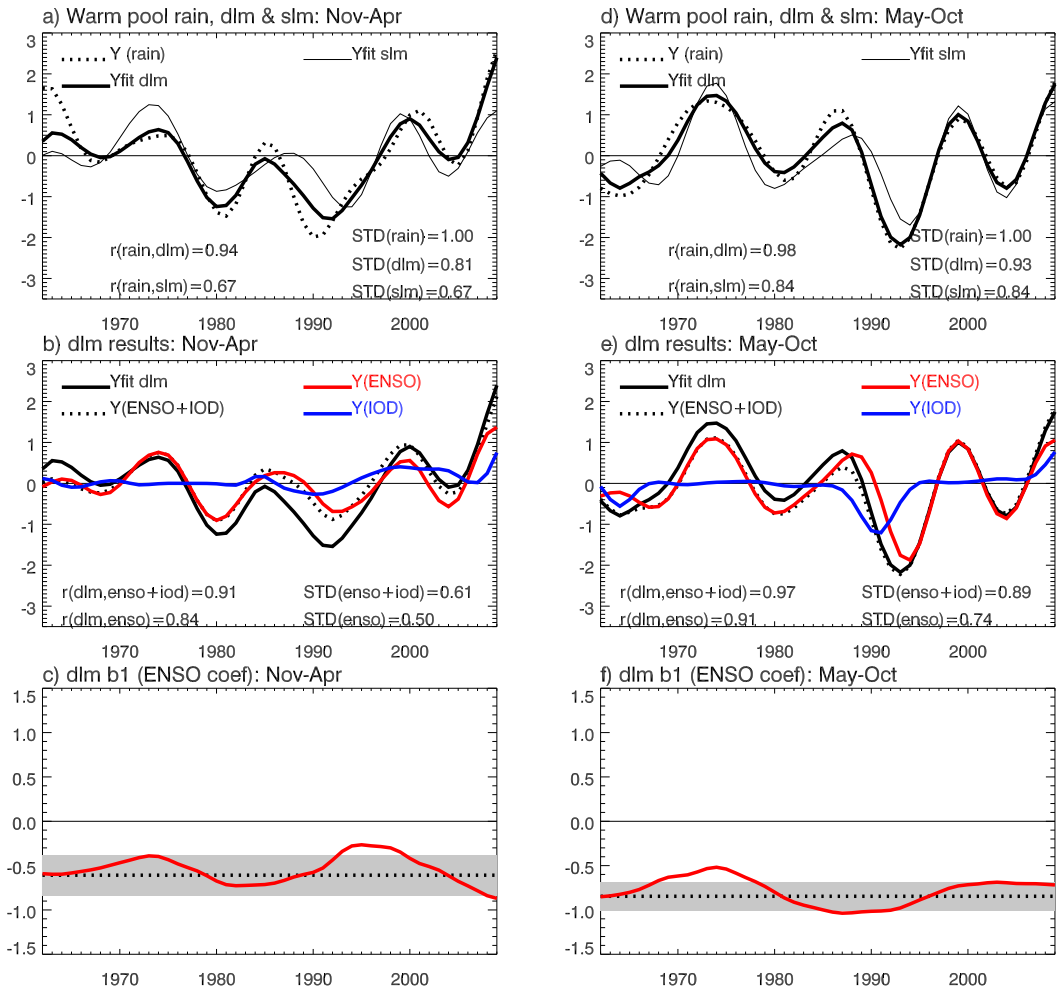

FIG. 12. As in Fig. 9, but for DLM results of 8-yr low-pass-filtered CRU precipitation averaged in the warm-pool region (boxed area in Fig. 2).

be highly nonlinear and stochastic in nature (e.g., Wunsch 1999; Stephenson et al. 2000; Gershunov et al. 2001).

The dominant role played by ENSO decadal variability is the major cause for the significant covariability between the warm-pool convection and Indian–Pacific WCs during winter, and the covariability for the convection and Pacific WC during summer. The Indian Ocean WC and warm-pool convection, however, do not covary during summer, because the Indian Ocean WC is not controlled by ENSO; rather, it is also strongly influenced by the decadal IOD, Indian summer monsoon, and Indian Ocean SST (sections 4a and 4b).

5. Summary and discussion

In this paper, we carry out observational analyses to explore decadal variations of the Indian and Pacific Ocean WCs and warm-pool convection (Figs. 1 and 2) since the 1960s, examine their covariability, and elucidate their causes by applying a novel approach, the Bayesian DLM. Following existing studies that investigate the centennial and multidecadal trends of the Indo-Pacific WCs, we focus on examining their surface branches, which are represented by the observationally based WASWind and various reanalysis products. The warm-pool convection is represented by CRU precipitation over land instead of ICOADS cloudiness, owing to the higher correlations of decadal variability of CRU precipitation with satellite-observed OLR and GPCP precipitation for their overlapping period (section 3a).

The Indian and Pacific Ocean WCs, together with convection over the Indo-Pacific warm pool, exhibit significant decadal variability (Figs. 4–6). During the November–April Indonesian wet and Indian winter

monsoon dry season, the warm-pool convection covaries with both the Indian ($r = 0.71$) and Pacific ($r = 0.85$) Ocean WCs from 1962 to 2009, with enhanced convection corresponding to enhanced WCs. The Indian and Pacific Ocean WCs highly covary for this season ($r = 0.81$; Fig. 6). During the May–October Indonesian dry and Indian summer monsoon wet season, the covariability for the Pacific WC and warm-pool convection remains high ($r = 0.73$) but that for the Indian Ocean WC and convection is low ($r = 0.3$; Fig. 4), and the Indian and Pacific Ocean WCs are essentially uncorrelated (Fig. 6). Decadal variability of the Indian and Pacific Ocean WCs and the seasonality of their covariability are robust to cross-dataset differences. The WCs' decadal variations are also confirmed by the CCMP satellite winds and AVISO SSHA zonal gradients within the recent two decades (Figs. 5 and 7), and by the consistent variability of zonal gradients of the upper-700-m thermosteric sea level based on in situ observations before the satellite era (Figs. 5 and 8).

The observed decadal variability of the Indo-Pacific WCs can be largely explained by decadal variability of ENSO, IOD, Indian summer monsoon convection, and basin-mean SST of the tropical Indian Ocean. Since this paper focuses on examining decadal variability rather than multidecadal trend (section 1), the linear trend for 1962–2009 is removed from each climate index (Fig. 3). The high level of wintertime covariability between the Indian and Pacific Ocean WCs, as well as that between the WCs and warm-pool convection, results from the vital role played by ENSO decadal variability, which controls the decadal variability of the Pacific and Indian Ocean WCs and is also the most important factor for determining variability of the warm-pool convection (Figs. 9–12), with El Niño–like (La Niña–like) conditions weakening (enhancing) the convection and both WCs. Note that ENSO and IOD decadal variability can only explain 61% of the STD of warm-pool convection during the November–April Indonesian wet season (Fig. 12), and the residual cannot be explained by other climate indices. This result suggests that causes for the decadal variability of warm-pool precipitation during the strong wintertime convection season are complex, which can be highly nonlinear and stochastic.

During summer, while ENSO decadal variability still controls the Pacific WC and warm-pool convection and thus their covariability, the causes for the Indian Ocean WC are much more complex. Since the decadal variability of ENSO, the IOD, Indian Ocean SST, and Indian monsoon convection all affect the Indian Ocean WC, and the Indian summer monsoon has a slightly higher contribution to the STD compared to ENSO for the 1962–2009 period (0.47 vs 0.40; Figs. 10 and 11) and the monsoon has played a dominant role since the late 1990s (Figs. 10 and 11), the Indian Ocean WC does not covary with the Pacific WC and the warm-pool convection. Note that the effect of IOD decadal variability on the warm-pool convection is weak, compared to its effect on the Indian Ocean WC. The caveat is that the IOD effect on warm-pool convection could be underestimated, since we use CRU precipitation over land to represent warm-pool convection, which does not have data over the ocean. It is possible that the IOD can have a significant influence on convection over the eastern Indian Ocean within the warm pool, during the May–October season when it develops and reaches maturity. This point is supported by the higher correlation for IOD and ICOADS cloudiness than that for IOD and CRU precipitation (Fig. 4).

Decadal variability of ENSO and IOD may affect the WCs and warm-pool convection in a similar way to their effects at interannual time scale (e.g., Rasmusson and Carpenter 1982), as indicated by their negative DLM coefficients (Figs. 9, 10, and 12). What are the possible mechanisms for the decadal variations of Indian summer monsoon convection and Indian Ocean SST to affect the Indian Ocean WC? The positive DLM coefficient of the Indian Ocean SST indicates that a warm (cold) Indian Ocean intensifies (reduces) the Indian Ocean WC (Fig. 11) by increasing convection over the eastern Indian Ocean warm pool, consistent with earlier studies on seasonal–interannual time scales (e.g., Gadgil et al. 1984; Graham and Barnett 1987; Waliser et al. 1993). The negative DLM coefficient of Indian summer monsoon (Fig. 11d) suggests that stronger convection of the Indian summer monsoon drives stronger monsoon winds and enhanced equatorial easterly trades, leading to weakened Indian Ocean WC.

Is the controlling effect of decadal ENSO on the Pacific WC variability contradictory to the previous results, which suggested the influence of the Indian and Atlantic Ocean SSTA on the Pacific WC (e.g., Luo et al. 2012, Han et al. 2014b, and McGregor et al. 2014)? Note that here we examine the decadal variability for the 1962–2009 period, whereas the previous studies focused on the warming trends since the 1980s or 1990s, even though Han et al. (2014b) also discussed 10–20-yr variability. Additionally, it is possible that the Niño-3.4 index includes the Indian and Atlantic Ocean SSTA effects, which are aliased into the ''decadal ENSO'' effect in our DLM model, resulting in a somewhat overestimated effect of decadal ENSO. While the Bayesian DLM is an advanced and useful tool, it does not really provide the causality of decadal variability. After the statistically robust relationship is established, controlled model experiments must be done to achieve unambiguous

understanding of the causes for the dynamical (time evolving) impacts of decadal climate variability and associated mechanisms, which is extremely lacking for the Indian Ocean. Results from this study contribute to our understanding of decadal climate variations over the Indo-Pacific basin in the past few decades, shed light on the causes for the complexity of the Indian Ocean WC variability, which is likely more difficult to predict than the Pacific WC, and set a process context for future decadal prediction over the Indo-Pacific region.

Acknowledgments. Part of this work was completed when Weiqing Han was visiting NCAR during her sabbatical leave. She thanks CCR/NCAR for providing partial summer salary support. W. Han is supported by National Science Foundation (NSF) AGS-1446480, NASA OSTST NNX17AI63G, NASA OVWST NNX14AM68G, and National Monsoon Mission Directorate Award SSC-03-002 from the Government of India. G. A. Meehl and A. Hu are partly supported by the Regional and Global Climate Modeling Program (RGCM) of the U.S. Department of Energy's Office of Science (BER), Cooperative Agreement DE-FC02-97ER62402, and the National Science Foundation. Jessica Kenigson is supported by NASA Harriett G. Jenkins Graduate Fellowship Program Grant NNX13AR74H. The National Center for Atmospheric Research is sponsored by the National Science Foundation.

REFERENCES

Adler, R. F., and Coauthors, 2003: The version-2 Global Precipitation Climatology Project (GPCP) monthly precipitation analysis (1979–present). *J. Hydrometeor.*, **4**, 1147–1167, doi:10.1175/1525-7541(2003)004<1147:TVGPCP>2.0.CO;2.

Allan, R., and Coauthors, 2001: Is there an Indian Ocean dipole and is it independent of the El Niño–Southern Oscillation? *CLIVAR Exchanges*, No. 21, International CLIVAR Project Office, Southampton, United Kingdom, 18–22.

Annamalai, H., R. Murtugudde, J. Potemra, S.-P. Xie, P. Liu, and B. Wang, 2003: Coupled dynamics over the Indian Ocean: Spring initiation of the zonal mode. *Deep-Sea Res. II*, **50**, 2305–2330, doi:10.1016/S0967-0645(03)00058-4.

——, S. Xie, J. McCreary, and R. Murtugudde, 2005: Impact of Indian Ocean sea surface temperature on developing El Niño. *J. Climate*, **18**, 302–319, doi:10.1175/JCLI-3268.1.

Ashok, K., Z. Guan, and T. Yamagata, 2001: Impact of the Indian Ocean dipole on the decadal relationship between the Indian monsoon rainfall and ENSO. *Geophys. Res. Lett.*, **28**, 4499–4502, doi:10.1029/2001GL013294.

——, W.-L. Chan, T. Motoi, and T. Yamagata, 2004: Decadal variability of the Indian Ocean dipole. *Geophys. Res. Lett.*, **31**, L24207, doi:10.1029/2004GL021345.

Atlas, R., R. N. Hoffman, J. Ardizzone, S. M. Leidner, J. C. Jusem, D. K. Smith, and D. Gombos, 2011: A cross-calibrated, multiplatform ocean surface wind velocity product for meteorological and oceanographic applications. *Bull. Amer. Meteor. Soc.*, **92**, 157–174, doi:10.1175/2010BAMS2946.1.

Babyak, M. A., 2004: What you see may not be what you get: A brief, nontechnical introduction to overfitting in regression-type models. *Psychosom. Med.*, **66**, 411–421.

Balmaseda, M. A., A. Vidard, and D. L. T. Anderson, 2008: The ECMWF ocean analysis system: ORA-S3. *Mon. Wea. Rev.*, **136**, 3018–3034, doi:10.1175/2008MWR2433.1.

——, K. Mogensen, and A. T. Weaver, 2013: Evaluation of the ECMWF ocean reanalysis system ORAS4. *Quart. J. Roy. Meteor. Soc.*, **139**, 1132–1161, doi:10.1002/qj.2063.

Baquero-Bernal, A., M. Latif, and S. Legutke, 2002: On dipolelike variability of sea surface temperature in the tropical Indian Ocean. *J. Climate*, **15**, 1358–1368, doi:10.1175/1520-0442(2002)015<1358:ODVOSS>2.0.CO;2.

Chadwick, R., I. Boutle, and G. Martin, 2013: Spatial patterns of precipitation change in CMIP5: Why the rich do not get richer in the tropics. *J. Climate*, **26**, 3803–3822, doi:10.1175/JCLI-D-12-00543.1.

Deser, C., A. S. Phillips, and M. A. Alexander, 2010: Twentieth century tropical sea surface temperature trends revisited. *Geophys. Res. Lett.*, **37**, L10701, doi:10.1029/2010GL043321.

——, and Coauthors, 2012: ENSO and Pacific decadal variability in the Community Climate System Model version 4. *J. Climate*, **25**, 2622–2651, doi:10.1175/JCLI-D-11-00301.1.

Dijkstra, H. A., and J. D. Neelin, 1995: Ocean–atmosphere interaction and the tropical climatology. Part II: Why the Pacific cold tongue is in the east. *J. Climate*, **8**, 1343–1359, doi:10.1175/1520-0442(1995)008<1343:OAIATT>2.0.CO;2.

Du, Y., S.-P. Xie, G. Huang, and K. Hu, 2009: Role of air–sea interaction in the long persistence of El Niño–induced north Indian Ocean warming. *J. Climate*, **22**, 2023–2038, doi:10.1175/2008JCLI2590.1.

Ducet, N., P. Le Traon, and G. Reverdin, 2000: Global high-resolution mapping of ocean circulation from TOPEX/Poseidon and ERS-1 and-2. *J. Geophys. Res.*, **105**, 19 477–19 498, doi:10.1029/2000JC900063.

Duchon, C. E., 1979: Lanczos filtering in one and two dimensions. *J. Appl. Meteor.*, **18**, 1016–1022, doi:10.1175/1520-0450(1979)018<1016:LFIOAT>2.0.CO;2.

England, M. H., and Coauthors, 2014: Recent intensification of wind-driven circulation in the Pacific and the ongoing warming hiatus. *Nat. Climate Change*, **4**, 222–227, doi:10.1038/nclimate2106.

Folland, C., J. Renwick, M. Salinger, and A. Mullan, 2002: Relative influences of the interdecadal Pacific oscillation and ENSO on the South Pacific convergence zone. *Geophys. Res. Lett.*, **29**, 1643, doi:10.1029/2001GL014201.

Freeman, E., and Coauthors, 2017: ICOADS release 3.0: A major update to the historical marine climate record. *Int. J. Climatol.*, **37**, 2211–2232, doi:10.1002/joc.4775.

Gadgil, S., N. Joshi, and P. Joseph, 1984: Ocean–atmosphere coupling over monsoon regions. *Nature*, **312**, 141–143, doi:10.1038/312141a0.

Gershunov, A., N. Schneider, and T. Barnett, 2001: Low-frequency modulation of the ENSO–Indian monsoon rainfall relationship: Signal or noise? *J. Climate*, **14**, 2486–2492, doi:10.1175/1520-0442(2001)014<2486:LFMOTE>2.0.CO;2.

Graham, N., and T. Barnett, 1987: Sea surface temperature, surface wind divergence, and convection over tropical oceans. *Science*, **238**, 657–659, doi:10.1126/science.238.4827.657.

Han, W., J. P. McCreary, D. L. T. Anderson, and A. J. Mariano, 1999: Dynamics of the eastward surface jets in the equatorial Indian Ocean. *J. Phys. Oceanogr.*, **29**, 2191–2209, doi:10.1175/1520-0485(1999)029<2191:DOTESJ>2.0.CO;2.

——, and Coauthors, 2010: Patterns of Indian Ocean sea-level change in a warming climate. *Nat. Geosci.*, **3**, 546–550, doi:10.1038/ngeo901.

——, J. Vialard, M. J. McPhaden, T. Lee, Y. Masumoto, M. Feng, and W. P. De Ruijter, 2014a: Indian Ocean decadal variability: A review. *Bull. Amer. Meteor. Soc.*, **95**, 1679–1703, doi:10.1175/BAMS-D-13-00028.1.

——, and Coauthors, 2014b: Intensification of decadal and multi-decadal sea level variability in the western tropical Pacific during recent decades. *Climate Dyn.*, **43**, 1357–1379, doi:10.1007/s00382-013-1951-1.

Hastenrath, S., 2002: Dipoles, temperature gradients, and tropical climate anomalies. *Bull. Amer. Meteor. Soc.*, **83**, 735–738, doi:10.1175/1520-0477(2002)083<0735:WLACNM>2.3.CO;2.

Ishii, M., and M. Kimoto, 2009: Reevaluation of historical ocean heat content variations with time-varying XBT and MBT depth bias corrections. *J. Oceanogr.*, **65**, 287–299, doi:10.1007/s10872-009-0027-7.

Jin, F.-F., 2001: Low-frequency modes of tropical ocean dynamics. *J. Climate*, **14**, 3874–3881, doi:10.1175/1520-0442(2001)014<3874:LFMOTO>2.0.CO;2.

Jones, P., and I. Harris, 2013: CRU TS3. 20: Climatic Research Unit (CRU) time-series (TS) version 3.20 of high resolution gridded data of month-by-month variation in climate (January 1901–December 2011). NCAS British Atmospheric Data Centre, accessed 20 June 2016, http://catalogue.ceda.ac.uk/uuid/3f8944800cc48e1cbc29a5ee12d8542d.

Kalnay, E., and Coauthors, 1996: The NCEP/NCAR 40-Year Reanalysis Project. *Bull. Amer. Meteor. Soc.*, **77**, 437–471, doi:10.1175/1520-0477(1996)077<0437:TNYRP>2.0.CO;2.

Karnauskas, K. B., R. Seager, A. Kaplan, Y. Kushnir, and M. A. Cane, 2009: Observed strengthening of the zonal sea surface temperature gradient across the equatorial Pacific Ocean. *J. Climate*, **22**, 4316–4321, doi:10.1175/2009JCLI2936.1.

Kennedy, J. J., N. A. Rayner, R. O. Smith, D. E. Parker, and M. Saunby, 2011a: Reassessing biases and other uncertainties in sea-surface temperature observations since 1850: 1. Measurement and sampling errors. *J. Geophys. Res.*, **116**, D14103, doi:10.1029/2010JD015218.

——, ——, ——, ——, and ——, 2011b: Reassessing biases and other uncertainties in sea-surface temperature observations since 1850: 2. Biases and homogenization. *J. Geophys. Res.*, **116**, D14104, doi:10.1029/2010JD015220.

Kitoh, A., H. Endo, K. Krishna Kumar, I. F. A. Cavalcanti, P. Goswami, and T. Zhou, 2013: Monsoons in a changing world: A regional perspective in a global context. *J. Geophys. Res. Atmos.*, **118**, 3053–3065, doi:10.1002/jgrd.50258.

Klein, S. A., B. J. Soden, and N.-C. Lau, 1999: Remote sea surface temperature variations during ENSO: Evidence for a tropical atmospheric bridge. *J. Climate*, **12**, 917–932, doi:10.1175/1520-0442(1999)012<0917:RSSTVD>2.0.CO;2.

Kobayashi, S., and Coauthors, 2015: The JRA-55 Reanalysis: General specifications and basic characteristics. *J. Meteor. Soc. Japan*, **93**, 5–48, doi:10.2151/jmsj.2015-001.

Krishnamurthy, V., and B. P. Kirtman, 2003: Variability of the Indian Ocean: Relation to monsoon and ENSO. *Quart. J. Roy. Meteor. Soc.*, **129**, 1623–1646, doi:10.1256/qj.01.166.

Krishnan, R., and P. Swapna, 2009: Significant influence of the boreal summer monsoon flow on the Indian Ocean response during dipole events. *J. Climate*, **22**, 5611–5634, doi:10.1175/2009JCLI2176.1.

Krishnaswamy, J., S. Vaidyanathan, B. Rajagopalan, M. Bonell, M. Sankaran, R. S. Bhalla, and S. Badiger, 2015: Non-stationary and non-linear influence of ENSO and Indian Ocean Dipole on the variability of Indian monsoon rainfall and extreme rain events. *Climate Dyn.*, **45**, 175–184, doi:10.1007/s00382-014-2288-0.

Kucharski, F., I.-S. Kang, R. Farneti, and L. Feudale, 2011: Tropical Pacific response to 20th century Atlantic warming. *Geophys. Res. Lett.*, **38**, L03702, doi:10.1029/2010GL046248.

——, F. S. Syed, A. Burhan, I. Farah, and A. Gohar, 2015: Tropical Atlantic influence on Pacific variability and mean state in the twentieth century in observations and CMIP5. *Climate Dyn.*, **44**, 881–896, doi:10.1007/s00382-014-2228-z.

Kumar, K. K., B. Rajagopalan, and M. A. Cane, 1999: On the weakening relationship between the Indian monsoon and ENSO. *Science*, **284**, 2156–2159, doi:10.1126/science.284.5423.2156.

Levitus, S., and Coauthors, 2012: World Ocean heat content and thermosteric sea level change (0–2000 m) 1955–2010. *Geophys. Res. Lett.*, **39**, L10603, doi:10.1029/2012GL051106.

L'Heureux, M. L., S. Lee, and B. Lyon, 2013: Recent multi-decadal strengthening of the Walker circulation across the tropical Pacific. *Nat. Climate Change*, **3**, 571–576, doi:10.1038/nclimate1840.

Li, X., S.-P. Xie, S. T. Gille, and G. Yoo, 2016: Atlantic-induced pan-tropical climate change over the past three decades. *Nat. Climate Change*, **6**, 275–279, doi:10.1038/nclimate2840.

Liebmann, B., and C. A. Smith, 1996: Description of a complete (interpolated) outgoing longwave radiation dataset. *Bull. Amer. Meteor. Soc.*, **77**, 1275–1277.

Livezey, R. E., and W. Chen, 1983: Statistical field significance and its determination by Monte Carlo techniques. *Mon. Wea. Rev.*, **111**, 46–59, doi:10.1175/1520-0493(1983)111<0046:SFSAID>2.0.CO;2.

Luo, J.-J., W. Sasaki, and Y. Masumoto, 2012: Indian Ocean warming modulates Pacific climate change. *Proc. Natl. Acad. Sci. USA*, **109**, 18 701–18 706, doi:10.1073/pnas.1210239109.

Mantua, N. J., S. R. Hare, Y. Zhang, J. M. Wallace, and R. C. Francis, 1997: A Pacific interdecadal climate oscillation with impacts on salmon production. *Bull. Amer. Meteor. Soc.*, **78**, 1069–1079, doi:10.1175/1520-0477(1997)078<1069:APICOW>2.0.CO;2.

McGregor, S., A. Timmermann, M. F. Stuecker, M. H. England, M. Merrifield, F.-F. Jin, and Y. Chikamoto, 2014: Recent Walker circulation strengthening and Pacific cooling amplified by Atlantic warming. *Nat. Climate Change*, **4**, 888–892, doi:10.1038/nclimate2330.

Meehl, G. A., 1987: The annual cycle and interannual variability in the tropical Pacific and Indian Ocean regions. *Mon. Wea. Rev.*, **115**, 27–50, doi:10.1175/1520-0493(1987)115<0027:TACAIV>2.0.CO;2.

——, and J. M. Arblaster, 2002: The tropospheric biennial oscillation and Asian–Australian monsoon rainfall. *J. Climate*, **15**, 722–744, doi:10.1175/1520-0442(2002)015<0722:TTBOAA>2.0.CO;2.

——, and A. Hu, 2006: Megadroughts in the Indian monsoon region and southwest North America and a mechanism for associated multi-decadal Pacific sea surface temperature anomalies. *J. Climate*, **19**, 1605–1623, doi:10.1175/JCLI3675.1.

——, J. M. Arblaster, and J. Loschnigg, 2003: Coupled ocean–atmosphere dynamical processes in the tropical Indian and Pacific Oceans and the TBO. *J. Climate*, **16**, 2138–2158, doi:10.1175/2767.1.

Meng, Q., M. Latif, W. Park, N. S. Keenlyside, V. A. Semenov, and T. Martin, 2012: Twentieth century Walker circulation change: Data analysis and model experiments. *Climate Dyn.*, **38**, 1757–1773, doi:10.1007/s00382-011-1047-8.

Minobe, S., 1997: A 50–70 year climatic oscillation over the North Pacific and North America. *Geophys. Res. Lett.*, **24**, 683–686, doi:10.1029/97GL00504.

Newman, M., 2013: Atmospheric science: Winds of change. *Nat. Climate Change*, **3**, 538–539, doi:10.1038/nclimate1915.

Osthus, D. A., 2015: Applications of and extensions to state-space models. Ph.D. dissertation, Iowa State University, 169 pp., http://lib.dr.iastate.edu/etd/14623/.

Parthasarathy, B., A. A. Munot, and D. R. Kothawale, 1995: Monthly and seasonal rainfall series for all-India homogeneous regions and meteorological subdivisions: 1871–1994. Indian Institute of Tropical Meteorology Research. Rep. RR-065, 113 pp.

Petris, G., 2010: dlm: Bayesian and likelihood analysis of dynamic linear models. R package version 1.1-1, http://CRAN.R-project.org/package=dlm.

——, S. Petrone, and P. Campagnoli, 2009: Dynamic linear models. *Dynamic Linear Models with R*, G. Petris, S. Petrone, and P. Campagnoli, Eds., Springer, 31–84.

Power, S., T. Casey, C. Folland, A. Colman, and V. Mehta, 1999: Inter-decadal modulation of the impact of ENSO on Australia. *Climate Dyn.*, **15**, 319–324, doi:10.1007/s003820050284.

Rasmusson, E. M., and T. H. Carpenter, 1982: Variations in tropical sea surface temperature and surface wind fields associated with the Southern Oscillation/El Niño. *Mon. Wea. Rev.*, **110**, 354–384, doi:10.1175/1520-0493(1982)110<0354:VITSST>2.0.CO;2.

Rayner, N. A., P. Brohan, D. E. Parker, C. K. Folland, J. J. Kennedy, M. Vanicek, T. Ansell, and S. F. B. Tett, 2006: Improved analyses of changes and uncertainties in marine temperature measured in situ since the mid-nineteenth century: The HadSST2 dataset. *J. Climate*, **19**, 446–469, doi:10.1175/JCLI3637.1.

R Development Core Team, 2016: R: A language and environment for statistical computing. R Foundation for Statistical Computing, https://www.R-project.org/.

Rio, M. H., S. Guinehut, and G. Larnicol, 2011: New CNES-CLS09 global mean dynamic topography computed from the combination of GRACE data, altimetry, and in situ measurements. *J. Geophys. Res.*, **116**, C07018, doi:10.1029/2010JC006505.

Saji, N., B. Goswami, P. Vinayachandran, and T. Yamagata, 1999: A dipole mode in the tropical Indian Ocean. *Nature*, **401**, 360–363.

Shankar, D., and Coauthors, 2010: Minima of interannual sea-level variability in the Indian Ocean. *Prog. Oceanogr.*, **84**, 225–241, doi:10.1016/j.pocean.2009.10.002.

Smith, T. M. and R. W. Reynolds, 2004: Improved extended reconstruction of SST (1854–1997). *J. Climate*, **17**, 2466–2477, https://doi.org/10.1175/1520-0442(2004)017<2466:IEROS>2.0.CO;2.

Solomon, A., and M. Newman, 2012: Reconciling disparate twentieth-century Indo-Pacific ocean temperature trends in the instrumental record. *Nat. Climate Change*, **2**, 691–699, doi:10.1038/nclimate1591.

Song, Q., G. A. Vecchi, and A. J. Rosati, 2007: Indian Ocean variability in the GFDL coupled climate model. *J. Climate*, **20**, 2895–2916, doi:10.1175/JCLI4159.1.

Stephenson, D. B., V. Pavan, and R. Bojariu, 2000: Is the North Atlantic Oscillation a random walk? *Int. J. Climatol.*, **20**, 1–18, doi:10.1002/(SICI)1097-0088(200001)20:1<1::AID-JOC456>3.0.CO;2-P.

Sun, S., J. Lan, Y. Fang, and X. Gao, 2015: A triggering mechanism for the Indian Ocean dipoles independent of ENSO. *J. Climate*, **28**, 5063–5076, doi:10.1175/JCLI-D-14-00580.1.

Tokinaga, H., and S.-P. Xie, 2011: Wave- and Anemometer-Based Sea Surface Wind (WASWind) for climate change analysis. *J. Climate*, **24**, 267–285, doi:10.1175/2010JCLI3789.1.

——, ——, C. Deser, Y. Kosaka, and Y. M. Okumura, 2012a: Slowdown of the Walker circulation driven by tropical Indo-Pacific warming. *Nature*, **491**, 439–443, doi:10.1038/nature11576.

——, ——, A. Timmermann, S. McGregor, T. Ogata, H. Kubota, and Y. M. Okumura, 2012b: Regional patterns of tropical Indo-Pacific climate change: Evidence of the Walker circulation weakening. *J. Climate*, **25**, 1689–1710, doi:10.1175/JCLI-D-11-00263.1.

Torrence, C., and P. J. Webster, 1999: Interdecadal changes in the ENSO–monsoon system. *J. Climate*, **12**, 2679–2690, doi:10.1175/1520-0442(1999)012<2679:ICITEM>2.0.CO;2.

Tozuka, T., J.-J. Luo, S. Masson, and T. Yamagata, 2007: Decadal modulations of the Indian Ocean dipole in the SINTEX-F1 coupled GCM. *J. Climate*, **20**, 2881–2894, doi:10.1175/JCLI4168.1.

Turner, A. G., and H. Annamalai, 2012: Climate change and the South Asian summer monsoon. *Nat. Climate Change*, **2**, 587–595, doi:10.1038/nclimate1495.

Vecchi, G. A., and B. J. Soden, 2007: Global warming and the weakening of the tropical circulation. *J. Climate*, **20**, 4316–4340, doi:10.1175/JCLI4258.1.

——, ——, A. T. Wittenberg, I. M. Held, A. Leetmaa, and M. J. Harrison, 2006: Weakening of tropical Pacific atmospheric circulation due to anthropogenic forcing. *Nature*, **441**, 73–76, doi:10.1038/nature04744.

Waliser, D. E., N. E. Graham, and C. Gautier, 1993: Comparison of the highly reflective cloud and outgoing longwave radiation datasets for use in estimating tropical deep convection. *J. Climate*, **6**, 331–353, doi:10.1175/1520-0442(1993)006<0331:COTHRC>2.0.CO;2.

Walker, G. T., and E. W. Bliss, 1937: World weather VI. *Mem. Roy. Meteor. Soc.*, **4**, 119–139.

Wang, C., C. Deser, J.-Y. Yu, P. DiNezio, and A. Clement, 2016: El Niño and Southern Oscillation (ENSO): A review. *Coral Reefs of the Eastern Pacific*, P. Glynn, D. Manzello, and I. Enochs, Eds., Springer, **4**, 85–106, doi:10.1007/978-94-017-7499-4_4.

Webster, P. J., A. M. Moore, J. P. Loschnigg, and R. R. Leben, 1999: Coupled ocean–atmosphere dynamics in the Indian Ocean during 1997–98. *Nature*, **401**, 356–360, doi:10.1038/43848.

Wentz, F. J., J. Scott, R. Hoffman, M. Leidner, R. Atlas, and J. Ardizzone, 2015: Remote Sensing Systems Cross-Calibrated Multi-Platform (CCMP) 6-hourly ocean vector wind analysis product on 0.25° grid, version 2.0. Remote Sensing Systems, accessed 15 April 2016, www.remss.com/measurements/ccmp.

Woodruff, S. D., and Coauthors, 2011: ICOADS release 2.5: Extensions and enhancements to the surface marine meteorological archive. *Int. J. Climatol.*, **31**, 951–967, doi:10.1002/joc.2103.

Wunsch, C., 1999: The interpretation of short climate records, with comments on the North Atlantic and Southern Oscillations. *Bull. Amer. Meteor. Soc.*, **80**, 245–255, doi:10.1175/1520-0477(1999)080<0245:TIOSCR>2.0.CO;2.

Xie, S.-P., H. Annamalai, F. A. Schott, and J. P. McCreary Jr., 2002: Structure and mechanisms of south Indian Ocean climate variability. *J. Climate*, **15**, 864–878, doi:10.1175/1520-0442(2002)015<0864:SAMOSI>2.0.CO;2.

——, Y. Du, G. Huang, X.-T. Zheng, H. Tokinaga, K. M. Hu, and Q. Y. Liu, 2010: Decadal shift in El Niño influences on Indo–western Pacific and East Asian climate in the 1970s. *J. Climate*, **23**, 3352–3368, doi:10.1175/2010JCLI3429.1.

Yamagata, T., S. K. Behera, S. A. Rao, Z. Guan, K. Ashok, and H. N. Saji, 2003: Comments on ''Dipoles, temperature gradients, and tropical climate anomalies.'' *Bull. Amer. Meteor. Soc.*, **84**, 1418–1422, doi:10.1175/BAMS-84-10-1418.

Yanto, B. Rajagopalan, and E. Zagona, 2016: Space–time variability of Indonesian rainfall at inter-annual and multi-decadal time scales. *Climate Dyn.*, **47**, 2975–2989, https://doi.org/10.1007/s00382-016-3008-8.

Yasunaka, S., and M. Kimoto, 2013: Upper ocean warming pattern in the past 50 years. *J. Oceanogr.*, **69**, 87–95, doi:10.1007/s10872-012-0159-z.

Yu, B., and F. W. Zwiers, 2010: Changes in equatorial atmospheric zonal circulations in recent decades. *Geophys. Res. Lett.*, **37**, L05701, doi:10.1029/2009GL042071.

Zhang, L., and K. B. Karnauskas, 2017: The role of tropical interbasin SST gradients in forcing Walker circulation trends. *J. Climate*, **30**, 499–508, doi:10.1175/JCLI-D-16-0349.1.

Zhang, X., and J. A. Church, 2012: Sea level trends, interannual and decadal variability in the Pacific Ocean. *Geophys. Res. Lett.*, **39**, L21701, doi:10.1029/2012GL053240.

Zhang, Y., J. M. Wallace, and D. S. Battisti, 1997: ENSO-like interdecadal variability: 1900–93. *J. Climate*, **10**, 1004–1020, doi:10.1175/1520-0442(1997)010<1004:ELIV>2.0.CO;2.